下させている．また，microsomal triglyceride transfer protein を低下させるため，超低比重リポ蛋白分泌を抑制し，細胞外への脂肪酸の放出を抑制している．さらに，HCV が誘発するインスリン抵抗性による高インスリン血漿は脂肪細胞からの肝細胞への遊離脂肪酸の取込みを増加させている．

HCV感染が宿主エネルギー代謝に与える影響

著者らは，JFH ウイルスを Huh-7 細胞に感染させ，感染がすべての細胞に広がった 9 日目に細胞のライセートを質量分析法でメタボローム解析を行った．その結果，クエン酸回路，プリン・ピリミジン合成系など蛋白核酸合成などは低下し，ATP，GTP，phosphocreatine などのエネルギー供与体は減少し，一方，解糖系は著明に亢進していた．クエン酸回路や電子伝達系を有し，生体内でエネルギー供給する ATP を産生する場所がミトコンドリアである．HCV 感染した細胞を電子顕微鏡で観察したところ，ミトコンドリアのクリステ構造が破壊されていた．さらに，螢光抗体法による観察では HCV 蛋白発現部位でミトコンドリア機能低下がみられた．このような HCV によるミトコンドリア障害はエネルギー産生低下をもたらす可能性がある．さらに，著者らは HCV 複製による細胞における ATP 消費量の変化を調べた[5]．レプリコン細胞から複製複合体を含む画分を分離し，ATP を添加しその減少量を比較したところ，オリジナルの細胞に比べて ATP 消費量が亢進していた．ATP が存在するとビーナスと CFP が結合し FRET 螢光を発する，ATP 濃度測定プローブ ATeam を用いて生細胞内の ATP の量と局在の解析をめざした．Ateam をレプリコン RNA の NS5A の下流に挿入することにより FRET 強度から ATP の量を評価するとともに，ドット状の螢光から複製複合体の局在を識別した．レプリコン細胞では複製複合体で強い FRET シグナルを観察した．著者らは，レプリコン細胞から複製複合体を粗精製し[2]，そこに含まれる HCV のゲノム複製に関与する宿主因子をプロテオミクスの手法を利用して探索し，creatine kinase B(CKB)を見出した[6]．CK は，エネルギーを多く必要とする，あるいは急速に必要とする組織での ATP の供給，ATP レベルの維持に重要であるとされており，CKB は NS4A との結合を介して HCV 複製複合体にリクルートされ，ATP を供給することで HCV 複製活性の維持に重要な役割を担っていると考えられた．

おわりに

HCV は感染した細胞に脂質を蓄積するという，HCV 増殖に好都合な環境をつくりだしているものと考えられる．また，感染細胞のメタボローム解析の結果，脂質代謝だけでなく，アミノ酸合成，RNA 核酸合成，TCA 回路，エネルギー産生系，糖新生・解糖系などに多彩な影響を与えている可能性が示された．このような解析は C 型肝炎患者の病態の理解につながると期待できる．

1) Roe, B. et al.: Metabolomic profile of hepatitis C virus-infected hepatocytes. *PLoS One*, **6**: e23641, 2011.
2) Aizaki, H. et al.: Characterization of the hepatitis C virus RNA replication complex associated with lipid rafts. *Virology*, **324**: 450-461, 2004.
3) Aizaki, H. et al.: Critical role of virion-associated cholesterol and sphingolipid in hepatitis C virus infection. *J. Virol.*, **82**: 5715-5724, 2008.
4) Moriya, K. et al.: Hepatitis C virus core protein induces hepatic steatosis in transgenic mice. *J. Gen. Virol.*, **78**: 1527-1531, 1997.
5) Ando, T. et al.: Visualization and Measurement of ATP Levels in Living Cells Replicating Hepatitis C Virus Genome RNA. *PLOS Pathogen.*, **8**: e1002561, 2012.
6) Hara, H. et al.: Involvement of creatine kinase B in hepatitis C virus genome replication through interaction with the viral NS4A protein. *J. Virol.*, **83**: 5137-5147, 2009.

相崎英樹／Hideki AIZAKI
国立感染症研究所ウイルス第二部

環境衛生

カドミウムを蓄積しないコメの開発

Newly developed rice that does not accumulate cadmium

日本人の食生活の特徴は米を主食とし，魚介類を多食することである．環境汚染物質の摂取源という観点からみると，日本人はおもに米からカドミウム(Cd)を摂取し，魚介類からメチル水銀やダイオキシン類を摂取している．Cd の消化管吸収率は 5%以下と低いが，体内に取り込まれるとおもに腎に蓄積し，その生物学的半減期は 20 年以上である．40 歳以上の日本人の腎には欧米諸国の 7〜8 倍にあたる 50〜100 μg/g の Cd が蓄積している(Cd が腎障害を起こす臨界濃度は 200 μg/g とされている)．

わが国では鉱山廃水に含まれる微量の Cd が現在なお水田を汚染している．しかも平成 23(2011)年には食品衛生法による米の Cd の安全基準が 1.0 ppm から 0.4 ppm に引き下げられた．日本人の主食である米の Cd 濃度を減少させる

SCIENTIFIC REPORTS

OPEN

SUBJECT AREAS:
MECHANISMS OF DISEASE
HEPATITIS C
LIVER FIBROSIS
TRANSFORMING GROWTH FACTOR BETA

Received
25 July 2013

Accepted
31 October 2013

Published
22 November 2013

Correspondence and requests for materials should be addressed to S.K. (skojima@riken.jp)

HCV NS3 protease enhances liver fibrosis via binding to and activating TGF-β type I receptor

Kotaro Sakata[1,2,3], Mitsuko Hara[1], Takaho Terada[4,5], Noriyuki Watanabe[6], Daisuke Takaya[4,7], So-ichi Yaguchi[8], Takehisa Matsumoto[4,7], Tomokazu Matsuura[9], Mikako Shirouzu[4,7], Shigeyuki Yokoyama[4,5], Tokio Yamaguchi[10], Keiji Miyazawa[8], Hideki Aizaki[6], Tetsuro Suzuki[11], Takaji Wakita[6], Masaya Imoto[2] & Soichi Kojima[1]

[1]Micro-signaling Regulation Technology Unit, RIKEN Center for Life Science Technologies, Saitama 351-0198, Japan, [2]Department of Biosciences and Informatics, Faculty of Science and Technology, Keio University, Kanagawa 223-8522, Japan, [3]Drug Discovery Laboratory, Wakunaga Pharmaceutical Co., Ltd., Hiroshima 739-1195, Japan, [4]RIKEN Systems and Structural Biology Center, Kanagawa 230-0045, Japan, [5]RIKEN Structural Biology Laboratory, Kanagawa 230-0045, Japan, [6]Department of Virology II, National Institute of Infectious Diseases, Tokyo 162-8640, Japan, [7]Division of Structural and Synthetic Biology, RIKEN Center for Life Science Technologies, Kanagawa 230-0045, Japan, [8]Department of Biochemistry, Interdisciplinary Graduate School of Medicine and Engineering, University of Yamanashi, Yamanashi 409-3898, Japan, [9]Department of Laboratory Medicine, the Jikei University School of Medicine, Tokyo 105-8461, Japan, [10]RIKEN Program for Drug Discovery and Medical Technology Platforms, Saitama 351-0198, Japan, [11]Department of Infectious Diseases, Hamamatsu University School of Medicine, Shizuoka 431-3192, Japan.

Viruses sometimes mimic host proteins and hijack the host cell machinery. Hepatitis C virus (HCV) causes liver fibrosis, a process largely mediated by the overexpression of transforming growth factor (TGF)-β and collagen, although the precise underlying mechanism is unknown. Here, we report that HCV non-structural protein 3 (NS3) protease affects the antigenicity and bioactivity of TGF-β2 in $(CAGA)_9$-Luc CCL64 cells and in human hepatic cell lines via binding to TGF-β type I receptor (TβRI). Tumor necrosis factor (TNF)-α facilitates this mechanism by increasing the colocalization of TβRI with NS3 protease on the surface of HCV-infected cells. An anti-NS3 antibody against computationally predicted binding sites for TβRI blocked the TGF-β mimetic activities of NS3 *in vitro* and attenuated liver fibrosis in HCV-infected chimeric mice. These data suggest that HCV NS3 protease mimics TGF-β2 and functions, at least in part, via directly binding to and activating TβRI, thereby enhancing liver fibrosis.

Viruses sometimes take over the host cell machinery by mimicking host cell proteins. This strategy infers survival, infection, and replication advantages to the virus[1,2], which may thereby contribute to the development of human disease.

Chronic hepatitis C virus (HCV) infection is one of the major causes of liver fibrosis, cirrhosis, and hepatocellular carcinoma[3,4]. However, the molecular mechanism by which HCV induces liver fibrosis is not fully understood. An estimated 130–170 million people worldwide are infected with HCV[5]. HCV, classified in the genus *Hepacivirus* of the family *Flaviviridae*, is a positive-strand RNA virus with an approximately 9.6-kb viral genome encoding structural (core, E1, and E2) and non-structural proteins (p7, NS2, NS3, NS4A, NS4B, NS5A, and NS5B)[6]. Of these proteins, NS3 is a member of the serine protease family that cleaves the HCV polyprotein to generate mature viral proteins that are required for viral replication[7].

Liver fibrosis, a common feature of chronic liver diseases, is caused by the excessive accumulation of extracellular matrix (ECM) proteins, including collagen. Transforming growth factor (TGF)-β, the most potent fibrogenic cytokine, is produced in its high molecular weight latent form and partly activated through the proteolytic cleavage of its propeptide region, termed latency associated protein (LAP), by serine proteases, plasmin, and plasma kallikrein[8,9]. The resultant active TGF-β signals via TGF-β type I (TβRI) and type II receptors (TβRII), inducing the phosphorylation of Smad2/3, which then binds to Smad4 and forms a complex that enters the cell nucleus. This complex acts as a transcription factor that controls the expression of target genes, including collagen and TGF-β itself, by binding to the DNA elements containing the minimal Smad-binding element, CAGA box[10].

Because the LAPs of TGF-β2 and -β3 have sequences that share partially homology with the NS3 cleavage site between NS3 and NS4A of HCV[7], we speculated that NS3 might activate TGF-β2 and/or TGF-β3 via the proteolytic cleavage of their LAP portions. We found, however, that NS3 protease DID NOT directly activate latent TGF-β2/3. Instead, it mimicked TGF-β2 and induced TGF-β signaling by binding and activating TβRI, leading to the induction of fibrogenic genes. This pathway was enhanced in the presence of an inflammatory cytokine, tumor necrosis factor (TNF)-α, as TNF-α increased the expression of TβRI. Furthermore, we found that NS3 colocalized with TβRI on the surface of an HCV-infected hepatoma cell line, and we observed direct binding between recombinant NS3 and TβRI. These phenomena were reproduced in chimeric mice transplanted with human hepatocytes that had been infected with HCV. These data suggest a novel mechanism by which HCV induces liver fibrosis.

Results

HCV NS3 protease exerted TGF-β mimetic activity via TβRI. To confirm whether HCV NS3 protease might induce the activation of latent TGF-β2, bacterially expressed recombinant NS3 (Supplementary Fig. S1) was incubated with conditioned medium obtained from HEK293T cells transiently overexpressing latent TGF-β2, and the concentration of active TGF-β2 in the reaction mixtures were measured by ELISA. Although the addition of NS3 increased active TGF-β2 concentrations in a dose-dependent manner, these increases were not time-dependent (Supplementary Fig. S2). Instead, we found that NS3 protease itself reacted with TGF-β2 in a dose-dependent manner, as determined by ELISA (Fig. 1A). Next, to assess whether NS3 could induce the bioactivity of TGF-β via TβRI, and whether its activity was dependent on protease activity, we performed a luciferase reporter assay with the TGF-β-responsive $(CAGA)_9$-Luc reporter in CCL64 cells. NS3 demonstrated TGF-β mimetic activity, which was alleviated in the presence of TβRI kinase inhibitors (SB-431542 and LY-364947) in a dose-dependent manner (Fig. 1B). In contrast, an NS3 protease inhibitor, VX-950 (telaprevir), did not affect luciferase activity (Fig. 1B). An unrelated protein with almost the same molecular weight as NS3, HLA class II histocompatibility antigen, DM α chain (HLA-DMA), as well as a carrier-free, tag-control sample, did not exert TGF-β mimetic activity, thus demonstrating the specificity of NS3 (Supplementary Fig. S3). Additionally, an anti-TGF-β2 antibody that detected NS3 in the TGF-β2 ELISA did not inhibit luciferase activity (Supplementary Fig. S4).

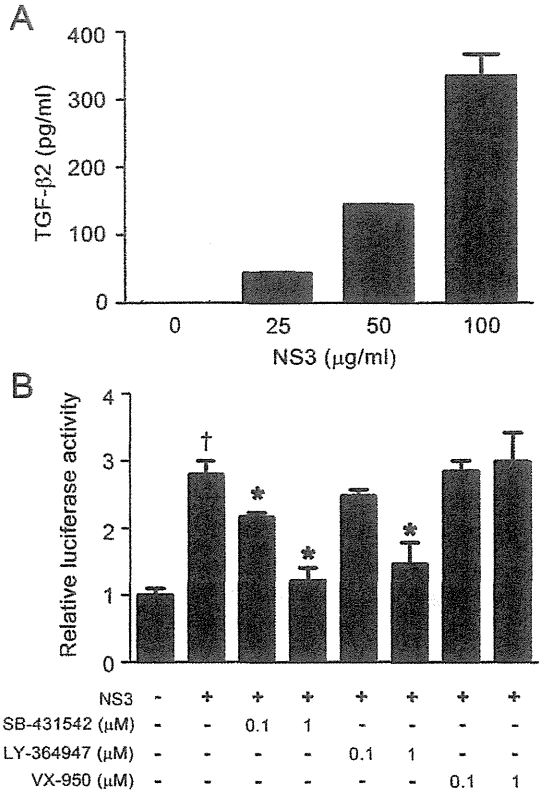

Figure 1 | HCV NS3 protease exerted TGF-β mimetic activity via the type I receptor. (A) TGF-β2 antigenicity of NS3. The indicated concentrations of recombinant NS3 protease were used in the TGF-β2 ELISA assays. (B) TGF-β mimetic activity of NS3 and its suppression by TβRI kinase inhibitors. $(CAGA)_9$-Luc CCL64 cells were stimulated with 100 μg/ml of recombinant NS3 protease for 24 hours, with or without the indicated concentration of TβRI kinase inhibitor or the NS3 protease inhibitor VX-950 (telaprevir). After 24 hours, the cells were harvested and luciferase activity measured. $\dagger p < 0.05$ compared with untreated control cells, $^*p < 0.05$ compared with NS3-treated cells without any inhibitors. The data are shown as the mean ± SD (n = 3), and representative results from three independent experiments with similar results are shown.

NS3 stimulated collagen production in hepatic cells, which was augmented by TNF-α. We examined the effect of NS3 on the expression of TGF-β1 and collagen α1 (I) in the human hepatic stellate cell line LX-2. Treatment with NS3 for 12 hours significantly increased both TGF-β1 (1.6-fold) and collagen α1 (I) (1.4-fold) expression in these cells (Fig. 2A). On the contrary, NS3 did not affect the expression of these genes in the normal hepatic cell line Hc. The pretreatment of the cells with tumor necrosis factor-α (TNF-α) enhanced increased TGF-β1 and collagen α1 (I) expression mediated by NS3 and was also accompanied by an increase in TGF-β receptor expression (Fig. 2B). Further increases in TβRI expression were not observed by combination treatment with TNF-α, suggesting that TNF-α increased TβRI expression, which may have enhanced the TGF-β mimetic activity of NS3 in these cells. Furthermore, Smad3 phosphorylation was also induced by NS3 in Hc cells that had been pretreated with TNF-α (Fig. 2D). A similar cooperativity between TNF-α and NS3 protease was not observed in LX-2 cells (Fig. 2C).

Interaction between NS3 and TβRI on the surface of HCV-infected HCC cells. NS3 was immunostained on the surface of HCV-infected Huh-7.5.1 cells both with and without permeabilization. In contrast, an ER marker, calnexin, was only positive after the permeabilization of the cells (Fig. 3A). To examine whether NS3 that was localized to the surface of HCV-infected Huh-7.5.1 cells interacted with TβRI, we performed co-immunostaining (Fig. 3B) and in situ proximity ligation assay (PLA) (Fig. 3C) using antibodies against NS3 and TβRI. Both results showed that NS3 was colocalized and formed a complex with TβRI on the cell surface. Because LX-2 cells (hepatic stellate cells) are not infected with HCV, the data were not recorded. We also co-cultured Huh-7.5.1 infected with HCV and LX-2 cells and examined them using *in situ* PLA. However, the interaction between NS3 protease and TβRI was not observed on the surface of LX-2 cells. Furthermore, we performed co-immunoprecipitation assays using recombinant NS3 and the extracellular domain of TβRI and TβRII. As shown in Figure 3D, FLAG-tagged NS3 bound to TβRI and TβRII, whereas FLAG-tag alone failed to interact with TGF-β receptors (Fig. 3D and Supplementary Fig. S5).

Docking simulation using the Katchalski-Katzir algorithm predicted that NS3 interacts with TβRI at three sites, T22-S42, T76-P96, and G120-S139, in NS3 and F55-M70, I72-V85, and C86-Y99 in TβRI, respectively (Fig. 3E, Table 1, and Supplementary Fig. S6). The predicted binding site peptides, particularly the peptide derived from site 3, completely blocked the interaction between NS3 and

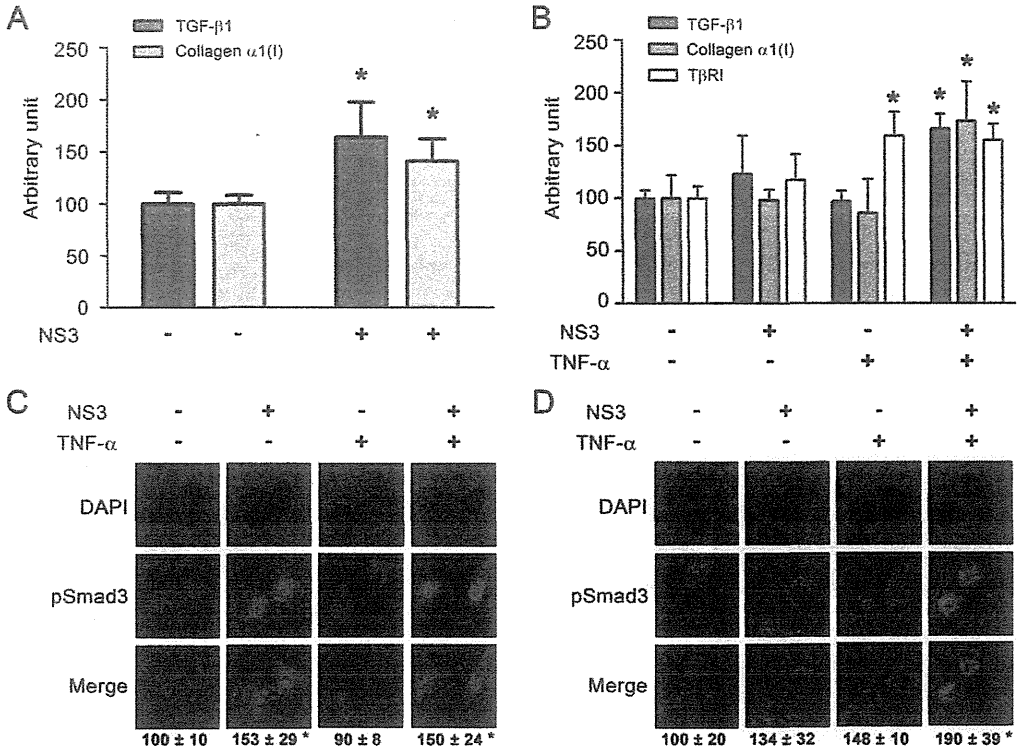

Figure 2 | **Cooperativity between NS3 and TNF-α in the stimulation of TGF-β1, collagen α1(I), and TβRI expression.** (A) Effect on TGF-β1 and collagen α1(I) mRNA expression in LX-2 cells. The cells were stimulated with 50 μg/ml of NS3 for 12 hours. Total cellular RNA was isolated and reverse transcribed to cDNA, and real-time PCR was performed as described in the Methods section. $*p < 0.05$ compared with untreated control cells. (B) Effect of pretreatment with TNF-α on the stimulation of expression of TGF-β1, collagen α1(I), and TβRI by NS3 protease in HC cells. Following the pretreatment of the cells with 20 ng/ml TNF-α for 12 hours, they were stimulated with 25 μg/ml NS3 for 12 hours, and mRNA expression was measured as described above. $*p < 0.05$ compared with untreated cells. The data are shown as the mean ± SD (n = 3). (C and D) The effect of pretreatment with TNF-α on the stimulation of phosphorylation of Smad3 by NS3 protease in LX-2 cells (C) and Hc cells (D). After the cells were treated with 20 ng/ml TNF-α for 12 hours and 25 μg/ml NS3 for another 12 hours, they were fixed, and immunofluorescent staining was performed as described in the Methods section. The experiments were performed in duplicate. The relative fluorescence intensities of phospho-Smad3 (% of untreated control cells) in 4 randomly selected fields from each dish were calculated with ZEN software and are shown as the mean ± SD. The results are representative of three independent experiments with similar results.

TβRI in the immunoprecipitation experiment (Supplementary Fig. S7A). Antibodies produced to these predicted binding sites within both NS3 and TβRI decreased the TGF-β mimetic activity of NS3 in $(CAGA)_9$-Luc CCL64 cells (Fig. 3F–H). Furthermore, the anti-NS3 antibody inhibited HCV-induced Smad3 phosphorylation (Supplementary Fig. S7B).

Anti-NS3 antibody prevented liver fibrosis in HCV-infected chimeric mice. To test our hypothesis that NS3 exerts TGF-β mimetic activity, thereby causing liver fibrosis, we examined whether the anti-NS3 antibody could prevent liver fibrosis in HCV-infected human hepatocyte-transplanted chimeric mice. The anti-NS3 antibody significantly prevented hepatic collagen accumulation in the mice (Fig. 4A) and decreased the mRNA expression of both TGF-β1 and collagen α1 (I) (Fig. 4B and 4C). There was no significant change in the serum levels of human albumin and HCV RNA during treatment with the anti-NS3 antibody (Supplementary Fig. S8A and S8B).

Discussion

Several groups have studied the molecular mechanisms by which HCV induces liver fibrosis and have reported the following: (i) HCV core protein activates the TGF-β1 promoter via the MAPK pathway in core protein-expressing human hepatocellular carcinoma HepG2 cells[11]; (ii) recombinant core protein upregulates the expression of fibrogenic genes in the human hepatic stellate cell line LX-2 via the toll-like receptor 2 [12] and the obese receptor[13]; and (iii) NS3 protease induces TGF-β1 production in NS3-overexpressing human hepatoma Huh-7 cells[14]. Our data show that NS3 protease mimics TGF-β2 and directly exerts its activity, at least in part, via binding to and activating TβRI, thereby enhancing liver fibrosis. The following experiments should be carried out in the future: effect of NS3 on TβRI phosphorylation, the expression of TGF-β2, TGF-β3, and other TGF-β responsive genes, such as plasminogen activator inhibitor-1, a tissue inhibitor of metalloproteinase-1, and α-smooth muscle actin, to further validate the TGF-β mimetic activity of NS3.

HCV NS3 is a chimera of a helicase and serine protease, which cleaves not only the junction between NS3-4A, NS4A-4B, NS4B-5A, and NS5A-5B for viral polyprotein processing, which is essential to the viral lifecycle, but also the toll-interleukin-1 receptor domain-containing, adaptor-inducing beta interferon, and mitochondrial antiviral signaling protein, which results in the disruption of innate immune responses[7,15]. An NS3 protease inhibitor, telaprevir, which was approved by the FDA in 2011, has been used in triple combination therapy with the current standard treatment of PEGylated interferon and ribavirin[16]. Telaprevir did not inhibit TGF-β mimetic activity in a $(CAGA)_9$-Luc reporter gene assay (Fig. 1C), suggesting that the TGF-β mimetic activity of NS3 is independent of its protease activity.

Much interest has centered on the fact that extraordinarily high concentrations of NS3 protease, up to 100 μg/ml, could exist in

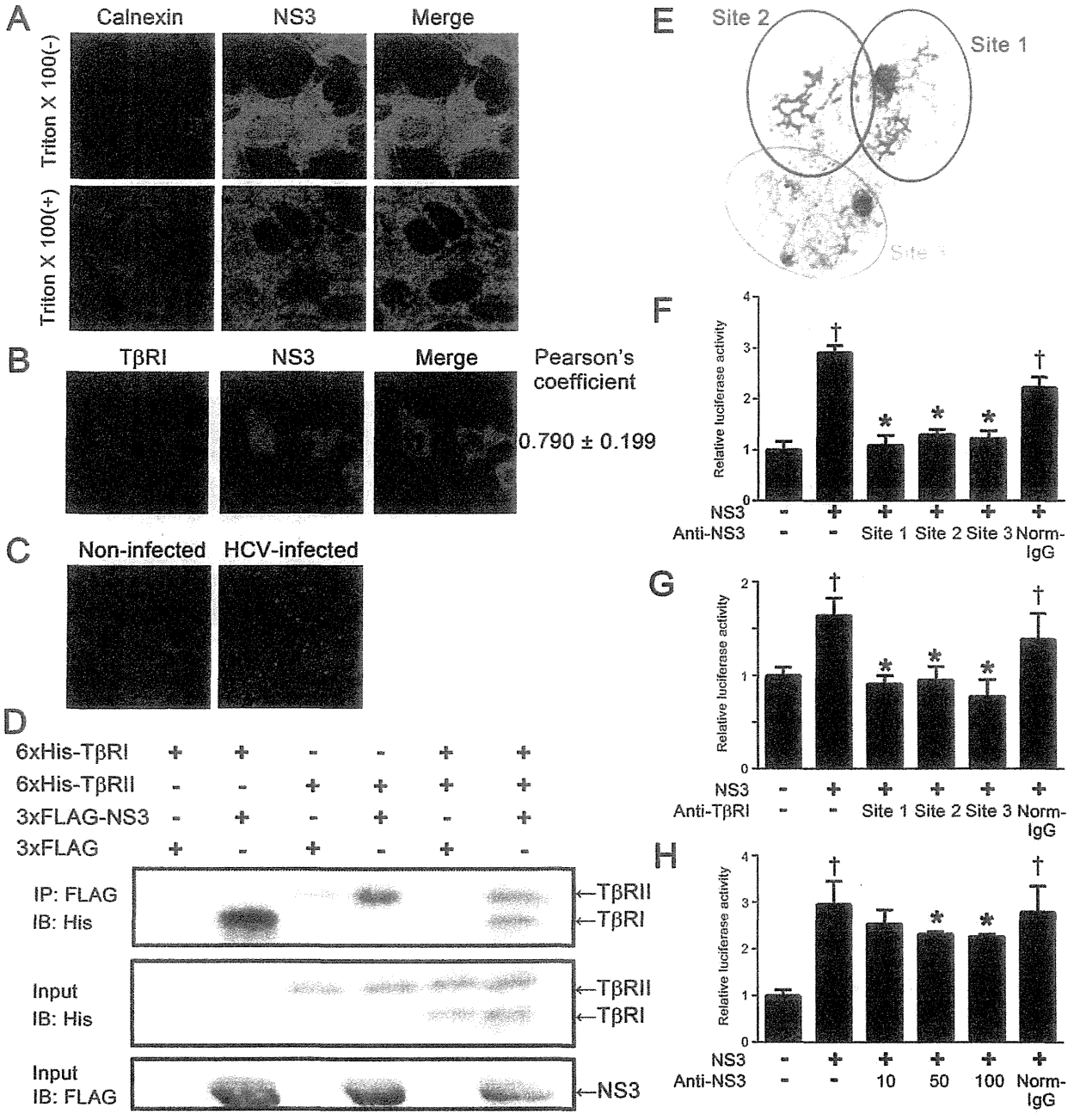

Figure 3 | NS3 protease colocalized and directly interacted with TβRI on the surface of HCV-infected cells. (A) The detection of NS3 protease on the surface of HCV-infected Huh-7.5.1 cells. The cells were fixed, followed ± by permeabilization with Triton-X 100, and then stained with DAPI, anti-NS3 antibody, and anti-calnexin antibody. (B) The colocalization of NS3 protease with TβRI in HCV-infected Huh7.5.1 cells. The cells were fixed and stained with DAPI, anti-NS3 antibody, and anti-TβRI antibody, as described in the Methods section. Pearson's colocalization coefficient values were obtained from 4 randomly selected fields using the ZEN software. The results are shown as the mean ± SD and are representative of three independent experiments with similar results. (C) The detection of NS3-TβRI proximity by in situ PLA in HCV-infected Huh-7.5.1 cells. The red dots indicate interactions between NS3 protease and TβRI, and the nuclei were identified by DAPI staining. (D) The physical interaction of NS3protease with TβRI and TβRII. FLAG-tagged NS3protease was incubated with 6xHis-tagged TβRI and/or TβRII and immunoprecipitated. The coprecipitated proteins were visualized by immunoblotting using anti-His antibody. The gels were run under the same experimental conditions. Cropped blots are shown (full-length blots are presented in Supplementary Fig. S5). (E) The structural overview of the NS3protease. The indicated colored amino acids (site 1, red; site 2, magenta; and site 3, cyan) show the important residues within the putative binding sites to TβRI, and the sequences are presented in Table 1. TGF-β mimetic activity of NS3 was inhibited in the presence of either anti-NS3 polyclonal antibodies against the predicted binding sites of TβRI (F), or anti-TβRI polyclonal antibodies against predicted binding sites of NS3 (G), and anti-NS3 monoclonal antibody against predicted binding site 3 of TβRI (H). Luciferase activities in $(CAGA)_9$-Luc CCL64 cells were measured as before. Normal mouse IgG (Norm-IgG) was used as a negative control. The data are shown as the mean ± SD. †$p < 0.05$ compared with untreated control cells, *$p < 0.05$ compared with NS3-treated cells without any antibodies. Representative results from three independent experiments with similar results are shown.

Table 1 | The amino acid sequences of predicted binding sites between NS3 protease and TβRI

	NS3 protease	TβRI
Site 1	TGRDKNQVEGEVQVVSTATQS	FVSVTETTDKVIHNSM
Site 2	TNVDQDLVGWPAPPGARSLTP	IAEIDLIPRDRPFV
Site 3	GDNRGSLLSPRPVSYLKGSS	CAPSSKTGSVTITTY

The underlined letters denote the putative contact residues.

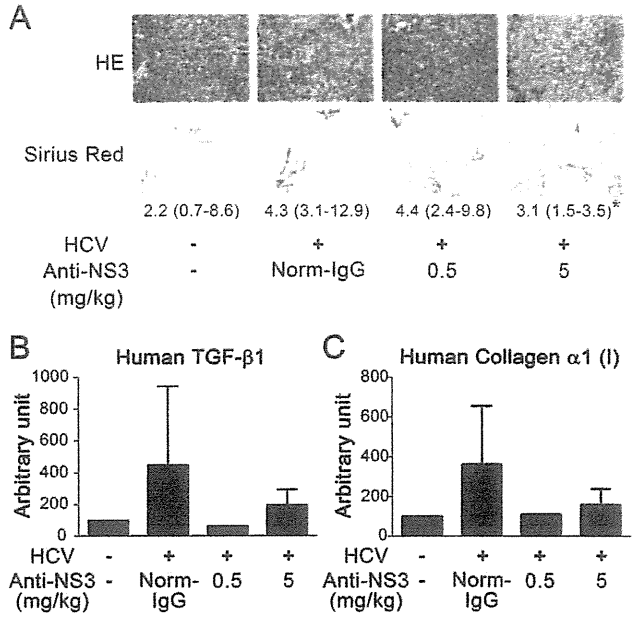

Figure 4 | Anti-NS3 antibody attenuated liver fibrosis in the HCV-infected chimeric mice. (A) Staining of liver sections. Paraffin sections were prepared from the livers of HCV-infected chimeric mice 16 weeks after HCV inoculation, and stained with hematoxylin and eosin (upper panels) and Sirius Red (lower panels). An anti-NS3 antibody was administered at the indicated doses, and normal mouse IgG (Norm-IgG) was administered at a dose of 5 mg/kg. For each group, the median ratios in Sirius Red positive/total area (%) from 6 randomly selected fields are shown, with the range in parentheses. $*p < 0.05$ compared with HCV-infected mice without anti-NS3 antibody. Scale bar = 100 μm. The representative result from 6 randomly selected fields is shown. (B) and (C) Hepatic mRNA expression in HCV-infected chimeric mice. Total RNA was isolated from the livers of these mice and reverse transcribed to cDNA, and real-time PCR was performed as described in the Methods section to quantitate the expression of human TGF-β1 expression (B) and human collagen α1 (I) (C). The data are shown as the mean ± SD, and representative results from two independent experiments with similar results are shown.

proximity to a TGF-β receptor. This line of inquiry led us to identify the cooperativity between NS3 and TNF-α, although the cooperative effect was maximal at one fourth this concentration of NS3. Serum levels of TNF-α in chronic hepatitis C patients are known to be significantly higher than those in healthy subjects[17,18]. We showed that TNF-α increased the susceptibility of cells to NS3 by enhancing the expression of TβRI, thereby further increasing the levels of profibrogenic genes (Fig. 2B). Various hepatic cell lines expressed different levels of TβRI, and there appeared to be a threshold in the level of TβRI that enabled cells to produce collagen mRNA upon stimulation with NS3. In particular, Hc cells expressed levels of TβRI below this predicted threshold (Supplementary Fig. S9). Consistent with our findings, carbon tetrachloride has recently been reported to induce acute liver injury, specifically significant liver fibrosis with inflammation, in transgenic mice expressing the full-length HCV polyprotein[19].

We documented the colocalization of NS3 and TβRI on the cell surface of HCV JFH-1-infected Huh-7.5.1 cells (Fig. 3). The results of co-immunoprecipitation and in situ PLA studies supported this conclusion. In future studies, we intend to use mutagenesis experiments of the predicted binding site and competition assays using NS3 and TGF-β in $(CAGA)_9$-Luc CCL64 cells to determine the mechanism of NS3 and TβRI binding. However, at present, how NS3 is released to the extracellular milieu remains to be elucidated. One possibility is that NS3 leaks passively from injured hepatocytes, as is the case for alanine aminotransferase and aspartate aminotransferase. Another possibility is that NS3 is secreted from HCV-infected cells via the Golgi complex. A recent report showed that nonstructural protein (NS) 1 of the dengue virus (DENV) and West Nile virus (WNV) is secreted from DENV- and WNV-infected cells through the Golgi complex following expression in association with the endoplasmic reticulum. Like HCV, these viruses are also members of the family *Flaviviridae*[20].

Zhang et al.[21] identified antibodies against NS3 in the serum of chronic hepatitis C patients and suggested that extracellular NS3 may be present in such cases. However, it remains unclear whether the concentration of HCV NS3 is as high as in our in vitro experiments. Although DENV NS1 has been reportedly detected at high levels (up to 50 μg/ml) in the serum of DENV-infected patients[22], further study is warranted to determine the serum or tissue NS3 concentrations in patients with chronic hepatitis C.

In this study, we generated polyclonal and monoclonal anti-NS3 antibodies that block the NS3-TβRI interaction. All anti-NS3 and anti-TβRI polyclonal antibodies generated against the predicted binding sites almost completely blocked TGF-β mimetic activity. This finding was likely due to steric hindrance by these antibodies or a requirement of binding at all three sites for signal transduction by NS3. The monoclonal antibody is a powerful tool that can be used to explore our working hypothesis that NS3 enhances liver fibrosis via the TGF-β receptor *in vivo*. We showed that the anti-NS3 monoclonal antibody generated against a predicted binding site to TβRI ameliorated liver fibrosis in HCV-infected human hepatocyte transplanted chimeric mice (Fig. 4A–C). The control of fibrosis after the eradication of the virus determines the prognosis, including the likelihood of progression to tumorigenesis. Therefore, the NS3 antibody against the TβRI binding site might have a clinical benefit in HCV patients with cirrhosis after combination therapy.

In conclusion, we demonstrated for the first time that HCV NS3 protease serves as a novel TGF-β receptor ligand and enhances liver fibrosis. This phenomenon might be beneficial to the virus, as TGF-β signals suppress host immunity. Our results provide elucidation regarding the molecular mechanism by which HCV induces liver fibrosis.

Methods

Materials. SB-431542 and LY-364947 were purchased from Sigma-Aldrich (St. Louis, MO). Recombinant human TNF-α was purchased from R&D systems, Inc. (Minneapolis, MN). Anti-NS3 antibody and anti-calnexin antibody were purchased from Abcam (Cambridge, UK). Anti-TβRI antibody and anti-phospho-Smad3 antibody were purchased from Santa Cruz Biotechnology (Santa Cruz, CA) and Immuno-Biological Laboratories (Gunma, Japan), respectively. Anti-Flag M2 antibody and anti-His antibody were purchased from Sigma (St. Louis, MO). Anti-NS3 antibodies and anti-TβRI antibodies against predicted binding sites were provided by the BioMatrix Research Institute (Chiba, Japan).

Cell culture. $(CAGA)_9$-Luc CCL64 cells were kindly provided by Prof. Hideaki Kakeya (Kyoto University, Kyoto, Japan), the hepatic stellate cell line LX-2 was kindly provided by Prof. Norifumi Kawada (Osaka City University, Osaka, Japan), and the human hepatoma cell line Huh-7.5.1 were maintained in Dulbecco's modified Eagle's medium (DMEM) supplemented with 10% fetal bovine serum, penicillin, and streptomycin. HC cells, a normal human hepatocyte cell line purchased from Cell Systems (Kirkland, WA), were cultured in CS-C complete medium (Kirkland, WA).

Protein preparation. The N-terminal histidine or 3xFLAG-tagged NS3 protease, and the extracellular domain of human TβRI and TβRII were expressed in *Escherichia coli* by isopropyl-β-thiogalactopyranoside induction. The protein was purified by affinity chromatography in a HisTrap HP column (GE Healthcare, Waukesha, WI). Detailed procedures are in the Supplementary information.

Enzyme-linked immunosorbent assay (ELISA). TGF-β2 ELISA was performed using a TGF-β2 Emax® Immune Assay System ELISA kit (Promega, Madison, WI) according to the manufacturer's instructions.

Luciferase assay. The mink lung epithelial cell line CCL64, which stably expressed $(CAGA)_9$-MLP-luciferase and contained nine copies of a Smad-binding CAGA box element upstream of a minimal adenovirus major late promoter (2×10^4 cells/well)[23], was seeded into 96-well plates. The next day, the medium was replaced with fresh medium containing 0.1% bovine serum albumin, and the cells were cultured for an additional 24 hours. The cells were extracted with lysis buffer, and luciferase activity was measured by a Luciferase Assay System (Promega, Madison, WI) according to the manufacturer's instructions.

Real-time RT-PCR. The isolation of total RNA and real-time RT-PCR were performed as described previously[24]. Briefly, total RNA was extracted using the RNeasy mini kit (Qiagen, Valencia, CA) according to the manufacturer's protocols. RNA (0.5 μg) was reverse transcribed to cDNA using the PrimeScript® RT Master Mix (Takara Bio Inc., Shiga, Japan). The mRNA expression levels were determined using real-time PCR. Real-time PCR was performed with the Thermal Cycler Dice® Real Time System, using the SsoAdvanced™ SYBR® Green Supermix (Bio-Rad Laboratories, Hercules, CA) and normalized to GAPDH mRNA expression. The primer sequences used were as follows: human TGF-β1 forward: 5′-ACT ATT GCT TCA GCT CCA CGG A-3′, reverse: 5′-GGT CCT TGC GGA AGT CAA TGT A-3′; human collagen α1 (I) forward: 5′-ACG AAG ACA TCC CAC CAA TC-3′, reverse: 5′-AGA TCA CGT CAT CGC ACA AC-3′; human GAPDH forward: 5′-GGA GTC AAC GGA TTT GGT-3′, reverse: 5′-AAG ATG GTG ATG GGA TTT CCA-3′; and human TβRI forward: 5′-CTT AAT TCC TCG AGA TAG GC-3′, reverse: 5′-GTG AGA TGC AGA CGA AGC-3′.

Immunofluorescence staining. The cells were grown on eight-well chamber slides or glass bottom dishes and were incubated with HCV virion for 24 hours at 37°C. The cells were washed with PBS, fixed with 4% paraformaldehyde for 10 min at room temperature, and permeabilized with 0.1% Triton X-100 for 20 min at room temperature. After blocking with 3% BSA/10% normal goat serum/PBS for 30 min, the cells were incubated with primary antibodies for 2 hours, followed by incubation with secondary antibodies for 30 min at RT. For detecting NS3 and TβRI on the cell surface, the cells were fixed without permeabilization after incubation with the secondary antibodies. After being washed with PBS, the cells were mounted with Vectashield DAPI mounting medium (Vector Laboratories, Inc., Burlingame, CA) and observed under a Zeiss LSM 700 laser scanning confocal microscope. For quantitative fluorescence analyses, the intensity of phosphorylated Smad3 and the colocalization of NS3 and TβRI (Pearson's colocalization coefficient values) in each panel were calculated with ZEN software.

Proximity ligation assay (PLA). HCV-infected Huh-7.5.1 cells were fixed with 4% paraformaldehyde for 10 min at room temperature and subjected to in situ PLA using a Duolink in situ red starter kit (Olink Bioscience, Uppsala, Sweden) according to the manufacturer's instructions. Briefly, cells were blocked and incubated with primary antibodies against NS3 and TβRI, followed by incubation with the PLA probes, which were secondary antibodies (anti-mouse and anti-rabbit) conjugated to oligonucleotides. DNA ligase was added to enable the formation of circular DNA strands when the PLA probes were in close proximity. This step was followed by incubation with oligonucleotides and polymerase for rolling circle amplification[25]. Texas red-labeled oligonucleotides, which hybridize to the amplified products, were used for visualization. The cells were observed under a Zeiss LSM 700 laser scanning confocal microscope.

Immunoprecipitation and immunoblotting. Anti-FLAG M2 affinity beads were pretreated with 5% bovine serum albumin in 20 mM Tris-HCl, pH 7.5, 150 mM NaCl overnight. Isotype control IgG was bound to Protein G PLUS-Agarose (Santa Cruz) pretreated with 5% bovine serum albumin in 20 mM Tris-HCl, pH 7.5, 150 mM NaCl. Cell lysates with 3xFLAG or 3x-FLAG-NS3 (2 mg protein) were incubated with 50 μl of the beads (10% slurry) at 4°C for 3 hours. The beads were then washed three times with the lysis buffer and incubated with lysates containing 6xHis-TβRI or 6xHis-TβRII (0.5 mg protein) at 4°C overnight. The bound proteins were eluted with the SDS-PAGE sample buffer after washing four times with the lysis buffer and then were subjected to SDS-PAGE (15% acrylamide) followed by transfer onto a PVDF membrane (Pall). The proteins were then visualized using anti-His tag HRP DirectT (MBL, 1/5000) or anti-FLAG BioM2 antibody (Sigma, 10 μg/ml) and horseradish peroxidase-conjugated anti-biotin antibody (Cell Signaling) using the ECL Western blotting detection reagent (GE Healthcare).

In silico docking simulation. The protein-protein docking simulation was implemented based on the geometric complementarity[26] between NS3 protease (PDB ID, 1NS3) and TβRI (PDB ID, 2PJY). Specifically, coordinates of the proteins were projected onto three-dimensional grids separated from each other at regular intervals. A surface score and an intramolecular score were assigned to each grid. This operation was conducted for both the receptor and the ligand. Next, convolution between the obtained grids was performed, the surfaces were explored exhaustively, and the complementarities of the binding states were calculated based on the scores. Amino acid residues appearing frequently in binding states with high complementarity scores can be estimated to be residues that are highly likely to appear in the interaction with an actual receptor. Accordingly, amino acid residues with an interatomic distance of 3.8 Å or less in the putative binding states were defined as contact residues and regarded as the putative contact residues of NS3 and TβRI.

Animal experiment. Chimeric mice with humanized livers were generated as previously described using urokinase-type plasminogen activator (uPA)-transgenic/SCID mice[27]. All mice were transplanted with frozen human hepatocytes obtained from a single donor. All animal experiments were approved by RIKEN Institutional Animal Use and Care Administrative Advisory Committees and were performed in accordance with RIKEN guidelines and regulations. Infection, extraction of serum samples, and euthanasia were performed under isoflurane anesthesia. Male chimeric mice (12- to 14-week old) were intravenously injected with 100 μl HCV J6/JFH-1 strain (1×10^8 copies/ml). Four weeks after HCV inoculation, anti-NS3 antibodies against predicted binding sites with the TβRI receptor were administered at doses of 0.5 mg/kg of BW or 5 mg/kg of BW twice a week for twelve weeks. Normal mouse IgG was administered at a dose of 5 mg/kg of BW as a control. When the animals were euthanized, the livers were either fixed with 4% paraformaldehyde for histological analysis or frozen immediately in liquid nitrogen for mRNA isolation.

Staining of liver tissue sections. The liver tissues were fixed in 4% paraformaldehyde and embedded in paraffin, and tissue sections (6 μm in thickness) were prepared with a Leica sliding microtome (Leica Microsystems, Nussloch, Germany). The liver tissue sections were deparaffinized, rehydrated, and incubated for 5 min with a drop of Proteinase K (Dako Envision) in 2 mL of 0.05 M Tris-HCl buffer (pH 7.5) at room temperature. The liver tissue sections were stained with Mayer's hematoxylin solution (Muto Chemicals) and 1% eosin Y solution (Muto Chemicals). Sirius Red, which results in a red staining of all fibrillar collagen, was used to evaluate fibrosis. Briefly, the liver sections were stained with 0.05% Fast Green FCF (ChemBlink, Inc. CAS: 2353-45-9) and 0.05% Direct Red 80 (Polysciences, Inc. CAS: 2610-10-18) in saturated picric acid (Muto Chemicals) for 90 min at room temperature. The ratios of Sirius Red positive/total area (%) from 6 randomly selected fields were measured for each group using WinROOF software (Mitani Corp., Tokyo, Japan).

Statistics. Statistical analysis was performed using one-way analysis of variance, followed by Dunnett's post-hoc test. A two-tailed Student's *t*-test was used to evaluate differences between the two groups. The Kruskal-Wallis test followed by Dunn's post-hoc test was used for multiple comparisons of Sirius Red positive areas.

1. Marazzi, I. *et al.* Suppression of the antiviral response by an influenza histone mimic. *Nature* **120**, 428–433 (2012).
2. Chaurushiya, M. S. *et al.* Viral E3 ubiquitin ligase-mediated degradation of a cellular E3: viral mimicry of a cellular phosphorylation mark targets the RNF8 FHA domain. *Mol. Cell.* **123**, 352–364 (2012).
3. Tong, M. J., el-Farra, N. S., Reikes, A. R. & Co, R. L. Clinical outcomes after transfusion-associated hepatitis C. *N. Engl. J. Med.* **332**, 1463–1466 (1995).
4. Poynard, T., Yuen, M. F., Ratziu, V. & Lai, C. L. Viral hepatitis C. *Lancet* **362**, 2095–2100 (2003).
5. Lavanchy, D. Chronic viral hepatitis as a public health issue in the world. *Best Pract Res Clin. Gastroenterol.* **22**, 991–1008 (2008).
6. Moradpour, D., Penin, F. & Rice, C. M. Replication of hepatitis C virus. *Nat. Rev. Microbiol.* **5**, 453–463 (2007).
7. Raney, K. D., Sharma, S. D., Moustafa, I. M. & Cameron, C. E. Hepatitis C virus non-structural protein 3 (HCV NS3): a multifunctional antiviral target. *J. Biol. Chem.* **285**, 22725–22731 (2010).
8. Okuno, M. *et al.* Prevention of rat fibrosis by protease inhibitor, Camostat Mesilate, via reduced generation of active TGF-β. *Gastroenterology* **120**, 1784–1800 (2001).
9. Akita, K. *et al.* Impaired liver regeneration in mice by lipopolysaccharide via TNF-α/kallikrein-mediated activation of latent TGF-β. *Gastroenterology* **123**, 352–364 (2002).
10. Ikushima, H. & Miyazono, K. TGFβ signalling: a complex web in cancer progression. *Nat. Rev. Cancer* **10**, 415–424 (2010).
11. Taniguchi, H. *et al.* Hepatitis C virus core protein upregulates transforming growth factor-β1 transcription. *J. Med. Virol.* **72**, 52–59 (2004).
12. Coenen, M. *et al.* Hepatitis C virus core protein induces fibrogenic actions of hepatic stellate cells via toll-like receptor 2. *Lab. Invest.* **91**, 1375–1382 (2011).
13. Wu, C. F., Lin, Y. L. & Huang, Y. T. Hepatitis C virus core protein stimulates fibrogenesis in hepatic stellate cells involving the obese receptor. *J. Cell. Biochem.* **114**, 541–550 (2012).
14. Presser, L. D., Haskett, A. & Waris, G. Hepatitis C virus-induced furin and thrombospondin-1 activate TGF-β1: Role of TGF-β1 in HCV replication. *Virology* **412**, 286–296 (2011).

15. Romano, K. P. *et al.* Molecular mechanisms of viral and host cell substrate recognition by hepatitis C virus NS3/4A protease. *J. Virol.* **85**, 6106–6116 (2011).
16. Kwong, A. D., Kauffman, R. S., Hurter, P. & Mueller, P. Discovery and development of telaprevir: an NS3-4A protease inhibitor for treating genotype 1 chronic hepatitis C virus. *Nat. Biotechnol.* **29**, 993–1003 (2011).
17. Toyoda, M. *et al.* Role of serum soluble Fas/soluble Fas ligand and TNF-α on response to interferon-α therapy in chronic hepatitis C. *Liver* **20**, 305–311 (2000).
18. Lecube, A., Hernandez, C., Genesca, J. & Simo, R. Proinflammatory cytokines, insulin resistance, and insulin secretion in chronic hepatitis C patients: A case-control study. *Diabetes Care* **29**, 1096–1101 (2006).
19. Chouteau, P. *et al.* Hepatitis C virus (HCV) protein expression enhances hepatic fibrosis in HCV transgenic mice exposed to a fibrogenic agent. *J. Hepatol.* **57**, 499–507 (2012).
20. Muller, D. A. & Young, P. R. The flavivirus NS1 protein: Molecular and structural biology, immunology, role in pathogenesis and application as a diagnostic biomarker. *Antiviral Res.* **98**, 192–208 (2013).
21. Zhang, Z. X., Sonnerborg, A. & Sallberg, M. A cell-binding Arg-Gly-Asp sequence is present in close proximity to the major linear antigenic region of HCV NS3. *Biochem. Biophys. Res. Commun.* **202**, 1352–1356 (1994).
22. Alcon, S. *et al.* Enzyme-linked immunosorbent assay specific to Dengue virus type 1 nonstructural protein NS1 reveals circulation of the antigen in the blood during the acute phase of disease in patients experiencing primary or secondary infections. *J. Clin. Microbiol.* **40**, 376–81 (2002).
23. Datta, P. K. & Moses, H. L. STRAP and Smad7 synergize in the inhibition of transforming growth factor beta signaling. *Mol. Cell. Biol.* **20**, 3157–3167 (2000).
24. Tatsukawa, H. *et al.* Role of transglutaminase 2 in liver injury via cross-linking and silencing of transcription factor Sp1. *Gastroenterology* **136**, 1783–1795 (2009).
25. Soderberg, O. *et al.* Characterizing proteins and their interactions in cells and tissues using the *in situ* proximity ligation assay. *Methods* **45**, 227–232 (2008).
26. Katchalski-Katzir, E. *et al.* Molecular surface recognition: determination of geometric fit between proteins and their ligands by correlation techniques. *Proc. Natl. Acad. Sci. USA* **89**, 2195–2199 (1992).
27. Tateno, C. *et al.* Near completely humanized liver in mice shows human-type metabolic responses to drugs. *Am. J. Pathol.* **165**, 901–912 (2004).

Acknowledgments

We are indebted to Mr. Kazushige Katsura and Ms. Chiemi Mishima-Tsumagari (RIKEN Systems and Structural Biology Center, Kanagawa, Japan; Division of Structural and Synthetic Biology, RIKEN Center for Life Science Technologies, Yokohama, Japan) for preparing and providing recombinant NS3, and Dr. Takashi Shimada, Dr. Chise Tateno, and Dr. Masakazu Kakuni (PhenixBio Co., Ltd., Hiroshima, Japan) for helpful discussions regarding the animal experiment. This work was supported in part by a Grant-in-Aid for Scientific Research from the Ministry of Education, Culture, Sports, Science and Technology (23390202 to S.K.), and Grants for Collaborative Researchers from Industries (to K.S.), Program for Drug Discovery and Medical Technology Platforms (to S.K.), and Chemical Genomics Research Program (to S.K.) from RIKEN.

Author contributions

Sakata K., Hara M. and Yaguchi S. performed experiments. Sakata K., Matsuura T., Miyazawa K., Imoto M. and Kojima S. wrote the manuscript. Terada T., Matsumoto T., Shirouzu M., Yokoyama S., Yamaguchi T. and Suzuki T. contributed to the production and the purification of recombinant NS3 and its antibodies. Watanabe N., Aizaki H. and Wakita T. contributed to the production and the purification of HCV and discussion from the point of view of virology. Takaya D. performed docking simulation to predict binding sites. Sakata K. and Kojima S. planned the research. Kojima S. supervised the entire project.

Additional information

Supplementary information accompanies this paper at http://www.nature.com/scientificreports

Competing financial interests: The authors declare no competing financial interests.

How to cite this article: Sakata, K. *et al.* HCV NS3 protease enhances liver fibrosis via binding to and activating TGF-β type I receptor. *Sci. Rep.* 3, 3243; DOI:10.1038/srep03243 (2013).

OPEN ACCESS Freely available online

PLOS | ONE

The Effect of Acyclic Retinoid on the Metabolomic Profiles of Hepatocytes and Hepatocellular Carcinoma Cells

Xian-Yang Qin[1,5], Feifei Wei[2,5], Masaru Tanokura[2], Naoto Ishibashi[3], Masahito Shimizu[4], Hisataka Moriwaki[4], Soichi Kojima[1]*

1 Micro-signaling Regulation Technology Unit, RIKEN Center for Life Science Technologies, Wako, Saitama, Japan, **2** Department of Applied Biological Chemistry, Graduate School of Agricultural and Life Sciences, University of Tokyo, Tokyo, Japan, **3** Tokyo New Drug Research Laboratories, Pharmaceutical Division, KOWA Company, Ltd., Tokyo, Japan, **4** Department of Gastroenterology, Gifu University Graduate School of Medicine, Gifu, Japan, **5** Japan Society for the Promotion of Science, Tokyo, Japan

Abstract

Background/Purpose: Acyclic retinoid (ACR) is a promising chemopreventive agent for hepatocellular carcinoma (HCC) that selectively inhibits the growth of HCC cells (JHH7) but not normal hepatic cells (Hc). To better understand the molecular basis of the selective anti-cancer effect of ACR, we performed nuclear magnetic resonance (NMR)-based and capillary electrophoresis time-of-flight mass spectrometry (CE-TOFMS)-based metabolome analyses in JHH7 and Hc cells after treatment with ACR.

Methodology/Principal Findings: NMR-based metabolomics revealed a distinct metabolomic profile of JHH7 cells at 18 h after ACR treatment but not at 4 h after ACR treatment. CE-TOFMS analysis identified 88 principal metabolites in JHH7 and Hc cells after 24 h of treatment with ethanol (EtOH) or ACR. The abundance of 71 of these metabolites was significantly different between EtOH-treated control JHH7 and Hc cells, and 49 of these metabolites were significantly down-regulated in the ACR-treated JHH7 cells compared to the EtOH-treated JHH7 cells. Of particular interest, the increase in adenosine-5'-triphosphate (ATP), the main cellular energy source, that was observed in the EtOH-treated control JHH7 cells was almost completely suppressed in the ACR-treated JHH7 cells; treatment with ACR restored ATP to the basal levels observed in both EtOH-control and ACR-treated Hc cells (0.72-fold compared to the EtOH control-treated JHH7 cells). Moreover, real-time PCR analyses revealed that ACR significantly increased the expression of pyruvate dehydrogenase kinases 4 (PDK4), a key regulator of ATP production, in JHH7 cells but not in Hc cells (3.06-fold and 1.20-fold compared to the EtOH control, respectively).

Conclusions/Significance: The results of the present study suggest that ACR may suppress the enhanced energy metabolism of JHH7 cells but not Hc cells; this occurs at least in part via the cancer-selective enhancement of PDK4 expression. The cancer-selective metabolic pathways identified in this study will be important targets of the anti-cancer activity of ACR.

Citation: Qin X-Y, Wei F, Tanokura M, Ishibashi N, Shimizu M, et al. (2013) The Effect of Acyclic Retinoid on the Metabolomic Profiles of Hepatocytes and Hepatocellular Carcinoma Cells. PLoS ONE 8(12): e82860. doi:10.1371/journal.pone.0082860

Editor: Matias A. Avila, University of Navarra School of Medicine and Center for Applied Medical Research (CIMA), Spain

Received August 11, 2013; **Accepted** November 6, 2013; **Published** December 23, 2013

Funding: This study was supported by the Japan Society for the Promotion of Science (JSPS) Postdoctoral Fellowship for Foreign Researchers. This study was also partly supported by the HMT Research Grant for Young Leaders in Metabolomics 2012 from Human Metabolome Technologies Inc. The funders had no role in the study design, data collection and analysis, decision to publish, or preparation of the manuscript.

Competing Interests: Co-author Naoto Ishibashi is employed by KOWA Company Ltd. This study was partly supported by the HMT Research Grant for Young Leaders in Metabolomics 2012 from Human Metabolome Technologies Inc. There are no patents, products in development or marketed products to declare. This does not alter the authors' adherence to all the PLOS ONE policies on sharing data and materials.

* E-mail: skojima@postman.riken.go.jp

Introduction

Hepatocellular carcinoma (HCC) represents approximately 85% of all primary liver cancers and is one of the most common malignancies worldwide, especially in Eastern Asia [1]. The prognosis of HCC remains very poor; this poor prognosis is due in part to its high rate of recurrence after initial treatment, which reaches approximately 70% within 5 years [2]. Acyclic retinoid (ACR), a synthetic retinoid with a vitamin A-like structure, prevents the recurrence and development of HCC in patients after the surgical removal of primary tumors [3,4]. ACR is currently undergoing phase II/III clinical trials (JapicCTI-121828) in Japan and is expected to become the first chemopreventive agent.

Another important characteristic of ACR is that it selectively suppresses the growth of HCC cells (JHH7 and others) but not normal hepatic cells (Hc) [5,6]. Although the mechanism underlying this effect is not fully understood, previous basic and clinical studies by our group and others have suggested that both non-genomic and genomic signaling pathways may be responsible for the cancer-selectivity of ACR [5,7,8,9,10,11,12]. A typical example is the prevention by ACR of the aberrant hyper-phosphorylation and inactivation of retinoid X receptor (RXR) α

that occurs during carcinogenesis in HCC [12] and the subsequent induction of apoptosis in HCC cells by the restoration of the expression of RXRα downstream genes such as p21 [11], transglutaminase 2 (TG2) [5] and more. However, to the best of our knowledge, no information is available regarding the effect of ACR on the metabolism of HCC cells.

Recently, the approach of targeting cancer metabolism to develop and improve cancer therapeutics has received a great deal of attention [13]. A distinguishing feature of cancer is that the metabolic pathways of cancer cells are adapted to support rapid and uncontrolled cell proliferation. One of the best-known alterations in cancer cell metabolism is a switch from mitochondrial oxidative phosphorylation to cytoplasmic glycolysis; this switch is known as the Warburg effect [14]. It is possible that targeting cellular metabolism may suppress cancer. In fact, several metabolism-targeting therapies have been already proven to be effective in the treatment of diverse human tumors [13,15].

Although chronic hepatitis B virus (HBV) or hepatitis C virus (HCV) infections are believed to account for approximately 80% of HCC [16], a growing body of evidence indicates that metabolic syndrome is also a risk factor for the development of HCC [17]. Indeed, it is extremely difficult to find a single essential target for cancer therapeutics, due to the remarkable heterogeneity and adaptability of cancer cells. It is likely that further investigations into the effect of ACR on cancer cell metabolism will improve our understanding of the molecular pathways underlying the cancer-selective growth suppressive effect of ACR and benefit the development of more effective cancer drugs and therapies against HCC. To achieve this, both nuclear magnetic resonance (NMR)-based and capillary electrophoresis time-of-flight mass spectrometry (CE-TOFMS)-based metabolome analyses were performed in JHH7 and Hc cells after treatment with ACR.

Materials and Methods

Materials

ACR (NIK-333) was supplied by Kowa Co. Ltd. (Tokyo, Japan). All-*trans*-retinoic acid (AtRA) was purchased from Sigma-Aldrich (St Louis, MO, USA). Ethanol (EtOH) was obtained from Wako Industries (Osaka, Japan), and used as the primary solvent for all reagents. EtOH solutions were further diluted into cell culture media for treatments. The final concentration of EtOH in media used as a control was 0.05% (vol/vol).

Cell culture

The JHH7 HCC cell line was kindly supplied by Dr. Matsuura (Jikei University School of Medicine, Tokyo, Japan) [18]. The normal human hepatocyte cell line (Hc) was purchased from Cell Systems (Kirkland, WA, USA). Both cell lines were maintained in Dulbecco's Modified Eagle Medium (DMEM; Wako Industries) containing 10% fetal bovine serum (FBS, Mediatech, Herndon, VA, USA), 100 U/ml penicillin/streptomycin and 2 mmol/L L-glutamine (Mediatech, Herndon, VA, USA) and grown at 37°C in a humidified 5% CO_2 incubator. For chemical treatment, the cells were cultured in serum-free media containing EtOH or ACR at the appropriate concentrations.

NMR-based metabolomics

For NMR analyses, cells (approximately 1×10^7 cells) treated with EtOH control or 10 μM ACR control for 4 h or 18 h were harvested by scraping as previously described [19]. The one-dimensional (1D) ^1H spectra were measured at 500 MHz on a Varian Unity INOVA-500 spectrometer. All NMR spectra were processed using the MestReNova program (Version 5.3.0, MestRec, Santiago de Compostela, Spain). Metabolites were identified using publicly accessible databases, including BioMagRes data bank (http://www.bmrb.wisc.edu), the Metabolomics Database of Linkoping (http://www.mdl.imv.liu.se), and the Human Metabolome Data Bank (http://www.hmdb.ca). Detailed NMR methods have been described previously [19,20].

CE-TOFMS analyses

JHH7 and Hc cells (approximately 5×10^6 cells) treated with EtOH control or 10 μM ACR for 24 h were washed twice with a 5% mannitol solution, and then 1,300 μL of a methanol solution containing 10 μM internal standards was added. Metabolome extraction was then performed as previously described [21]. The metabolic profiles of the cells were then measured using a CE-TOFMS-based metabolomics technique, which is a novel strategy for analyzing and differentially displaying metabolic profiles [21]. CE-TOFMS was carried out using an Agilent CE Capillary Electrophoresis System equipped with an Agilent 6210 Time-of-Flight mass spectrometer, Agilent 1100 isocratic HPLC pump, Agilent G1603A CE-MS adapter kit, and Agilent G1607A CE-ESI-MS sprayer kit (Agilent Technologies, Waldbronn, Germany).

Data analysis for CE-TOFMS and metabolite identification

The raw data obtained by CE-TOFMS were analyzed using KEIO MasterHands software exactly as previously described [22,23]. Briefly, the injected volume for CE and the sensitivity of MS were corrected using internal standards, and then all the annotated metabolites were further corrected to the same chemicals in a standard mixture to overcome different ionization patterns. The peaks were identified based on the matched mass-to-charge ratio (m/z) values and normalized migration times of the corresponding standard compounds.

Real-time RT-PCR

For PCR analyses, RNA was isolated from each cell culture treated with EtOH, AtRA or ACR for 4 h using an RNeasy Kit (Qiagen, Valencia, CA, USA), and the amount and purity of the isolated RNA were evaluated using a NanoDrop spectrophotometer (NanoDrop products, Wilmington, DE, USA). cDNA was then synthesized using a PrimeScript RT Master Mix Kit (TaKaRa Bio, Otsu, Japan). Oligonucleotide primers were designed using OligoPerfect Designer software (Invitrogen, Carlsbad, CA, USA; http://www.tools.invitrogen.com) and synthesized by Invitrogen. The sequences of the primers and the full gene names are summarized in Table S1. PCR reactions were performed using a the Thermal Cycler Dice™ Real Time System (TP8000; Takara Bio) with SsoAdvanced™ SYBR® Green Supermix (Bio-Rad Laboratories, Hercules, CA, USA).

Western blot analysis

JHH7 and Hc cells treated with EtOH, AtRA and ACR for 24 h were lysed using RIPA buffer. After boiling at 97°C for 10 min, the protein samples were resolved by sample buffer for sodium dodecyl sulfate (SDS) polyacrylamide gel electrophoresis, run on a 10% gel and transferred to a polyvinylidene difluoride membrane (Bio-Rad Laboratories). The membranes were blocked with 5% nonfat dry milk in Tris-buffered saline (TBS) and 0.1% Tween and then probed with primary antibodies against pyruvate dehydrogenase kinase 4 (PDK4; sc-14492; 1:1,000 dilution, Santa Cruz Biotechnology, CA, USA), pyruvate dehydrogenase (lipoamide) alpha 1 (PDHA1; sc-377092; 1:1,000 dilution, Santa Cruz Biotechnology), phospho-PDHA1 (ab92696; 1:1,000 dilution, Abcam) or Lamin B1 (ab16048; 1:5,000 dilution, Santa Cruz

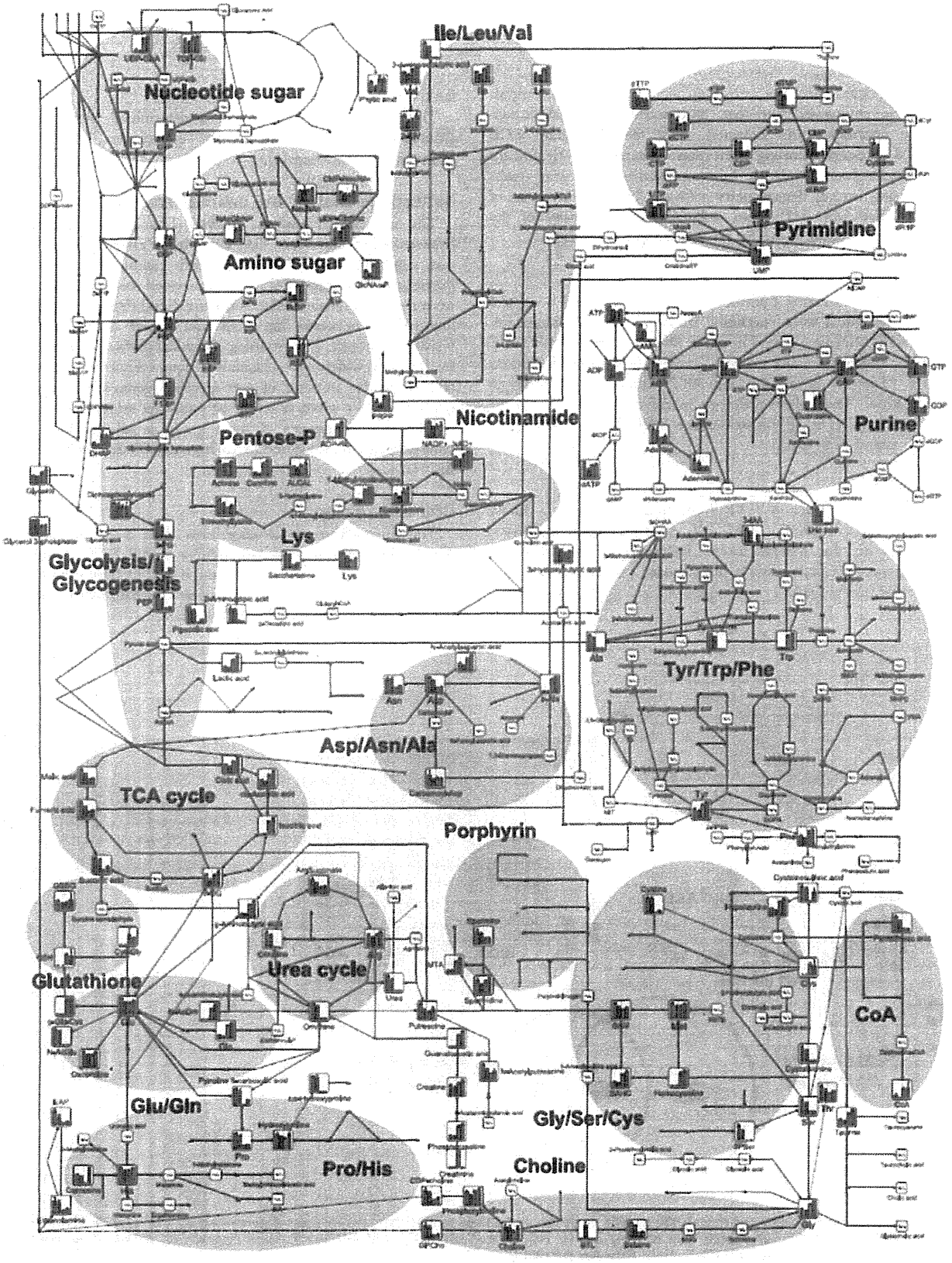
Ile/Leu/Val
Nucleotide sugar
Amino sugar
Pyrimidine
Nicotinamide
Pentose-P
Purine
Lys
Glycolysis/
Glycogenesis
Tyr/Trp/Phe
Asp/Asn/Ala
TCA cycle
Porphyrin
Glutathione
Urea cycle
CoA
Glu/Gln
Gly/Ser/Cys
Pro/His
Choline

Figure 1. Metabolites in the principle metabolic pathways of EtOH- or ACR-treated JHH7 and Hc cells detected by CE-TOFMS. The relative quantities of the detected metabolites are represented as bar graphs (from left to right: EtOH-treated JHH7, ACR-treated JHH7, EtOH-treated Hc, and ACR-treated Hc). N.D., not detected.
doi:10.1371/journal.pone.0082860.g001

Biotechnology). The blots were then incubated with horseradish peroxidase-conjugated anti-goat, anti-mouse or anti-rabbit secondary antibodies and detected using the Amersham ECL PlusTM Western Blotting Detection System (GE Healthcare UK, Buckingham, England). Immunoreactive bands were quantified using ImageJ densitometry software (National Institutes of Health, Bethesda, MD), and normalized; the density of the corresponding band in the EtOH control was set to 1.0.

RNA interference

An siRNA targeting human PDK4 (sc-39030) and a control siRNA (sc-37007) were purchased from Santa Cruz Biotechnology. JHH7 cells were plated in either 96-well plates (1×10^4 cells/well) for cell proliferation analysis and RNA isolation or 60-mm dishes (3.5×10^5 cells/dish) for ATP assays 1 day prior to transfection. The cells were then transfected with 50 nM or 100 nM siRNAs using Lipofectamine 2000 (Life Technologies, Grand Island, NY, USA).

ATP assay

The cellular levels of ATP were measured using a firefly bioluminescence assay kit (AMERIC-ATP kit, Wako Industries) according to the manufacturer's instructions. The luciferase activity was measured using a plate reader (ARVO MX, Perkin Elmer Inc., MA, USA).

Cell viability assay

The number of viable cells was determined using the Cell Counting Kit-8 (Dojindo Molecular Technologies, Tokyo, Japan) as previously described [5].

Network generation and pathway analyses

The Ingenuity Pathways Analysis (IPA) program (Ingenuity Systems, Mountain View, CA, USA; http://www.ingenuity.com) was used to identify networks and canonical pathways as previously described [24]. The generated biological networks were ranked by score, which is the likelihood that a set of genes is found in the networks due to random chance as measured by a Fisher's exact test. The resulting canonical pathways were ranked by *P* values, which were calculated using a Fisher's exact test by comparing the number of user-specified genes of interest that participate in a given function or pathway, relative to the total number of occurrences of these genes in all the functional/pathway annotations stored in the Ingenuity Pathways Knowledge Base [25].

GEO data mining

The normalized PDK4 expression from a clinical data set, which contains transcriptome profiling of 268 HCC tumor, 243 adjacent non-tumor, 40 cirrhotic and 6 healthy liver samples, was downloaded from the Gene Expression Omnibus (www.ncbi.nlm.nih.gov/geo, accession no. GSE25097).

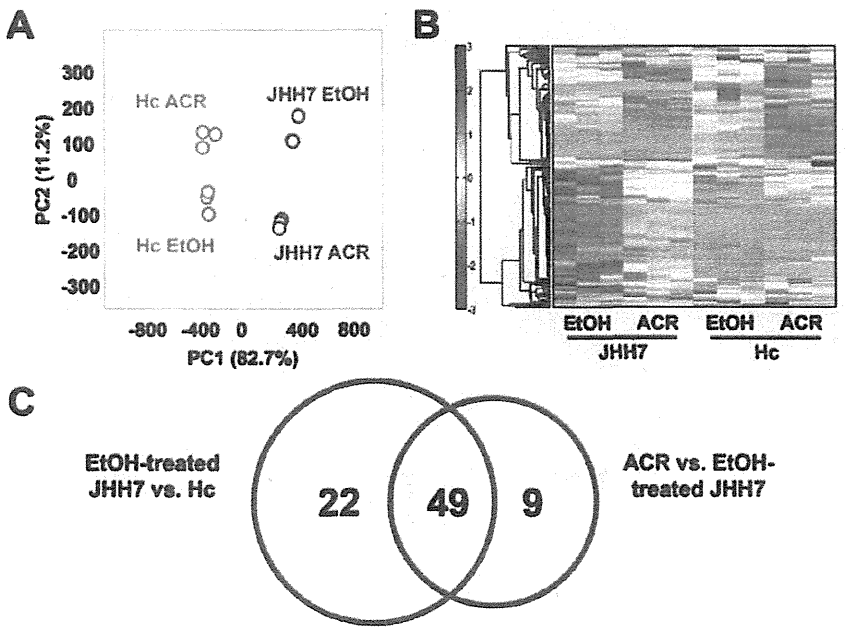

Figure 2. A comparison of the metabolic profile of EtOH- or ACR-treated JHH7 and Hc cells determined by CE-TOFMS. PCA scoreplot (*A*) and heat map (*B*) from metabolic data of JHH7 and Hc cells treated with EtOH and ACR ($n=3$). Venn-diagrams (*C*) showing the number of metabolites that were significantly deregulated between the two groups.
doi:10.1371/journal.pone.0082860.g002

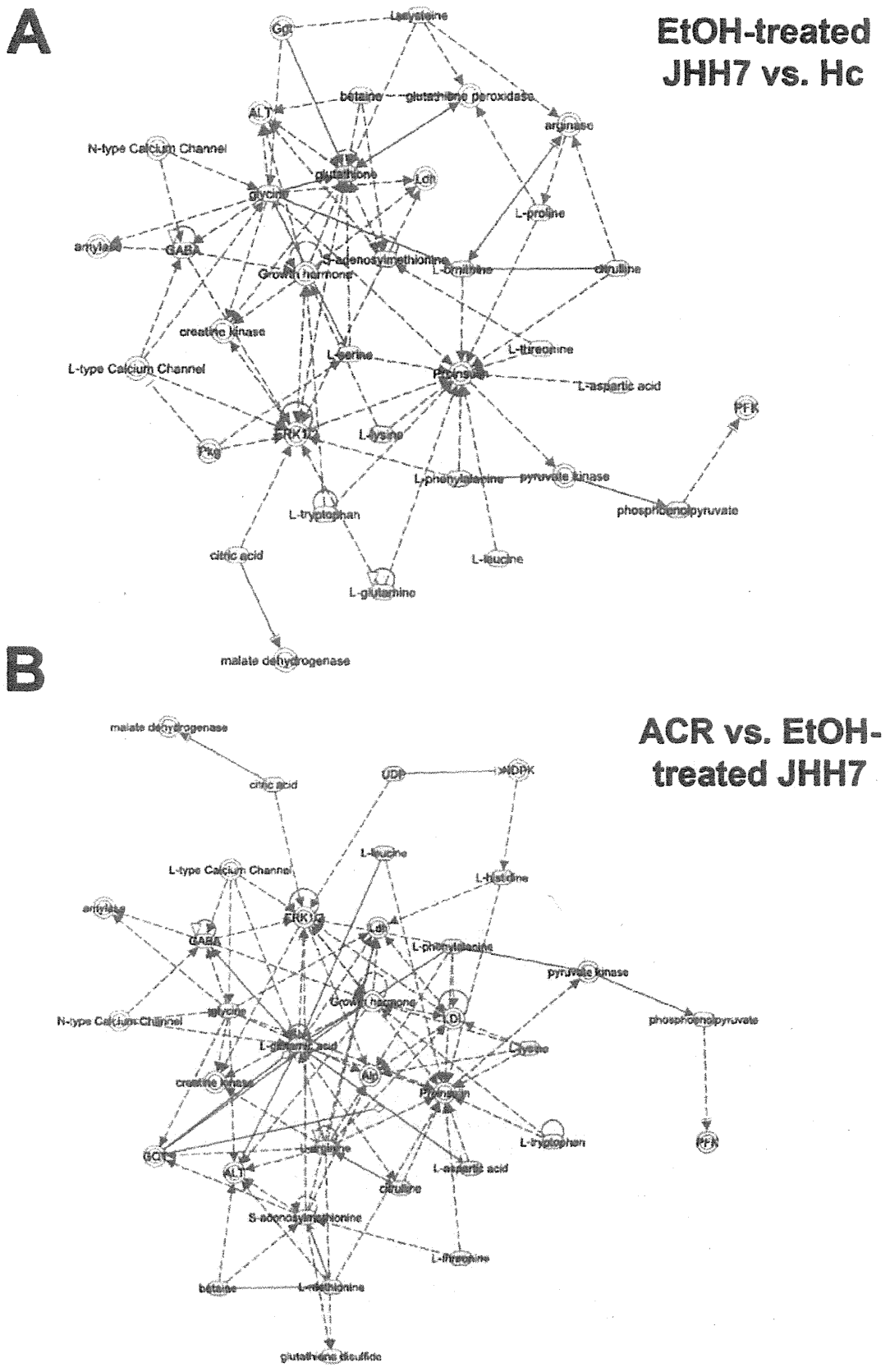
A
EtOH-treated JHH7 vs. Hc
Gpt
betaine
glutathione peroxidase
ALT
arginase
N-type Calcium Channel
glutathione
Ldh
glycine
L-proline
amylase
GABA
S-adenosylmethionine
L-ornithine
citrulline
Growth hormone
creatine kinase
L-serine
L-threonine
L-type Calcium Channel
Prolactin
L-aspartic acid
PFK
ERK1/2
L-lysine
Pka
L-phenylalanine
pyruvate kinase
L-tryptophan
phosphoenolpyruvate
citric acid
L-leucine
L-glutamine
malate dehydrogenase
B
ACR vs. EtOH-treated JHH7
malate dehydrogenase
citric acid
UDP
NDPK
L-leucine
L-type Calcium Channel
L-histidine
amylase
ERK1/2
GABA
Ldh
L-phenylalanine
pyruvate kinase
Growth hormone
N-type Calcium Channel
glycine
LDL
phosphoenolpyruvate
L-glutamic acid
L-lysine
creatine kinase
Ala
Prolactin
L-tryptophan
PFK
GOT
L-aspartic acid
ALT
citrulline
S-adenosylmethionine
L-threonine
betaine
L-methionine
glutathione disulfide

Figure 3. Network generation using Ingenuity Pathway Analysis. The "Increased Levels of Albumin, Amino Acid Metabolism, Molecular Transport" network was associated with metabolites that were significantly different between JHH7 and Hc cells (*A*) and the metabolites that were differentially regulated by ACR in JHH7 cells (*B*). Up-regulated metabolites are indicated in red, down-regulated metabolites indicated in green, and metabolites that were not annotated in this study but are part of this network are indicated in white. Direct relationships are drawn with solid arrows, and indirect relationships are drawn with dashed arrows.
doi:10.1371/journal.pone.0082860.g003

Statistical and multivariate analyses

All the experiments in this study were performed independently two or more times to ensure the reproducibility of the results. Quantitative data were expressed as the means ± SEMs. The statistical significance of differences between values was assessed using a two-tailed Student's *t*-test or a Mann-Whitney U test. Values of $P<0.05$ were considered to indicate statistical significance. Unsupervised principal component analysis (PCA) was run using SIMCA-P+ software (Version 12.0, Umetrics, Umeå, Sweden).

Results

The effect of ACR on the metabolism of JHH7 cells detected using ^{1}H-NMR

First, NMR-based metabolomics was performed to investigate the effect of ACR treatment on the metabolism of JHH7 cells. As shown in Figure S1, PCA analysis of the NMR spectra indicated that treatment with ACR for 4 h had a very minor effect on the metabolism of JHH7 cells, while obvious changes were observed after 18 h of ACR treatment compared to the EtOH control.

Differences between the metabolic profiles of JHH7 and Hc cells treated with EtOH and ACR detected using CE-TOFMS

To further investigate the cancer-selective effect of ACR, the metabolic profiles of JHH7 and Hc cells treated with EtOH and ACR for 24 h was measured using CE-TOFMS analysis. A total of 229 peaks (109 cationic and 120 anionic) were detected in either JHH7 or Hc cells; from these 229 peaks, 88 principal metabolites were quantified (Table S2). The metabolic pathways of all the detected metabolites are illustrated in Figure 1. These metabolites are associated with glycolysis/gluconegenesis, the pentose phosphate pathway, the tricarboxylic acid cycle, the urea cycle, pyrimidine metabolism, nicotinate and nicotinamide metabolism and amino acid metabolism. The result of the comparison of the metabolic profiles of the cells is provided in Figure 2. PCA analysis revealed a very clear distinction between the abundance of intracellular metabolites of JHH7 and Hc cells with and without ACR treatment (Figure 2A), while the first component (PC1) indicated that 67% of the total variance is due to the difference between JHH7 and Hc cells. PC2 (11.2%) indicated that the ACR-treated JHH7 cells have a metabolic profile that is similar to that of the EtOH-treated Hc cells. Furthermore, heatmap analyasis indicated that the metabolic pattern of JHH7 cells was almost completely opposite that of the Hc cells; a similar difference was observed between the ACR-treated and EtOH-treated JHH7 cells (Figure 2B). Finally, the cellular content of 71 metabolites in JHH7 and Hc cells was significantly different with *P* values less than 0.05 and fold changes greater than 1.2; 58 metabolites were significantly down-regulated by ACR in JHH7 cells compared to the EtOH control. Forty-nine common metabolites were shared between the two groups (Figure 2C).

Network generation and pathway analyses

Next, the list of the significantly different metabolites was imported into the IPA platform to investigate possible biological interactions. The biological functions of the top five IPA-generated networks and top five canonical metabolic pathways are summarized in Tables 1 and 2, respectively, and shown in Figure 3. Interestingly, IPA analysis indicated that the most highly populated biological network ("Increased Levels of Albumin, Amino Acid Metabolism, Molecular Transport") and the top two canonical metabolic pathways ("tRNA Charging" and "Purine Nucleotides De Novo Biosynthesis II") that were associated with the ACR-regulated metabolites by in JHH7 cells were the same as the networks that were associated with metabolic differences between JHH7 and Hc cells.

Table 1. Top five associated network functions generated by IPA.

	Top function	Score
EtOH-treated JHH7 vs. Hc	Increased Levels of Albumin, Amino Acid Metabolism, Molecular Transport	39
	Cellular Growth and Proliferation, Organismal Development, Cellular Compromise	21
	Cardiovascular System Development and Function, Organ Development, Carbohydrate Metabolism	18
	Cellular Growth and Proliferation, Organismal Development, Small Molecule Biochemistry	16
	Carbohydrate Metabolism, Cell Morphology, Cell-To-Cell Signaling and Interaction	11
ACR vs. EtOH-treated JHH7	Increased Levels of Albumin, Amino Acid Metabolism, Molecular Transport	38
	Carbohydrate Metabolism, Molecular Transport, Small Molecule Biochemistry	23
	Cellular Growth and Proliferation, Organismal Development, Small Molecule Biochemistry	16
	Free Radical Scavenging, Small Molecule Biochemistry, Molecular Transport	14
	Post-Translational Modification, Cellular Assembly and Organization, Developmental Disorder	6

doi:10.1371/journal.pone.0082860.t001

Table 2. Top canonical pathways identified by IPA.

	Top canonical pathway	P-Value
EtOH-treated JHH7 vs. Hc	tRNA Charging	6.82E-30
	Purine Nucleotides De Novo Biosynthesis II	1.30E-24
	Pyrimidine Ribonucleotides De Novo Biosynthesis	9.94E-20
	Superpathway of Citrulline Metabolism	9.93E-19
	Gluconeogenesis I	8.21E-18
ACR vs. EtOH-treated JHH7	tRNA Charging	9.48E-30
	Purine Nucleotides De Novo Biosynthesis II	2.91E-19
	Arginine Biosynthesis IV	3.10E-15
	Citrulline-Nitric Oxide Cycle	1.84E-14
	NAD biosynthesis II (from tryptophan)	5.72E-14

doi:10.1371/journal.pone.0082860.t002

ACR inhibits the increase in adenosine-5′-triphosphate (ATP) production in JHH7 cells

A comparison of the biosynthetic metabolites (nucleotides, amino acids and lipids) in the EtOH- or ACR-treated JHH7 and Hc cells determined by CE-TOFMS is summarized in Table 3. Of particular interest, the changes in the concentrations of adenosine nucleotides are shown in Figure 4. Notably, ATP levels were 1.6-fold higher in the EtOH-treated JHH7 cells than in the EtOH-treated Hc cells; ACR suppressed this increase, nearly to the basal levels observed in Hc cells (0.72-fold and $P=0.00015$ compared to the EtOH-treated JHH7 cells). In contrast, only a very minor effect of ACR was observed on the levels of adenosine diphosphate (ADP) and adenosine monophosphate (AMP) in JHH7 cells (0.84- and 0.82-fold compared to the EtOH control, respectively).

ACR enhances PDK4 expression in JHH7 cells, but not in Hc cells

To further understand the cancer-selective inhibitory effect of ACR on ATP production, a set of genes that is known to be important in the regulation of energy metabolism in cancer cells was selected based on previous reports [26,27,28,29], and the effect of ACR on the expression of these genes was measured using real-time PCR (Figure 5A). Of particular interest, we found that ACR significantly enhanced the expression of PDK4, an important regulator of ATP levels [30], in JHH7 cells but not in Hc cells (3.06-fold; $P=0.0033$ and 1.20-fold; $P=0.062$, respectively; Figure 5B). Further western blot analysis revealed a nearly 2-fold increase in PDK4 protein levels after ACR treatment, but ACR did not affect the phosphorylation of PDHA1 in JHH7 cells (Figure 5C).

Functional analysis of PDK4 in JHH7 cells

Furthermore, loss-of-function experiments were performed to confirm the role of PDK4 in the effect of ACR on cellular ATP levels and the proliferation of JHH7 cells. As shown in Figure 6A, treatment with an siRNA targeting PDK4 (siPDK4) caused a dose-dependent downregulation of PDK4 mRNA expression (0.57-fold and 0.41-fold compared to siControl-treated cells with 50 nM and 100 nM siPDK4, respectively). Interestingly, ACR weakly but significantly inhibited cellular ATP levels in siControl-treated JHH7 cells (0.88-fold and $P=0.042$ compared with EtOH). In contrast, no significant effect was observed in siPDK4-treated JHH7 cells (1.07-fold and $P=0.42$ compared with EtOH; Figure 6B). However, PDK4 knockdown did not rescue the inhibitory effect of ACR on the proliferation of JHH7 cells (Figure 6C).

Clinical expression levels of PDK4

The mining of microarray data from a human HCC data set revealed that PDK4 mRNA is significantly down-regulated in liver tumors compared to adjacent non-tumor liver tissues (0.66-fold, $P=3.11E-85$; Figure 7A). Finally, a PDK4-dependent regulatory network that involves RXR and peroxisome proliferator-activated

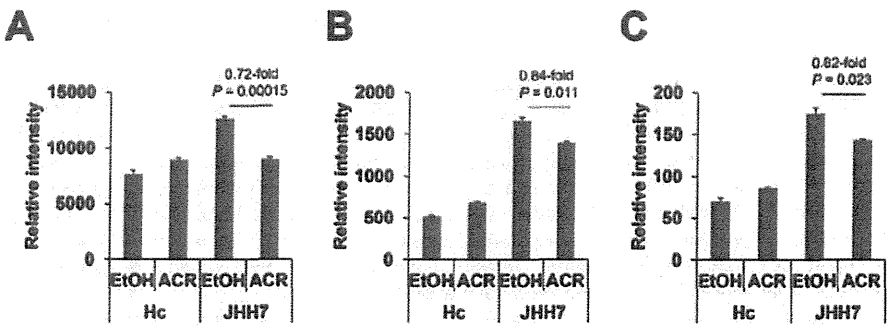

Figure 4. Levels of adenosine nucleotides in EtOH or ACR-treated JHH7 and Hc cells determined by CE-TOFMS. ATP (*A*), ADP (*B*) and AMP (*C*) levels.
doi:10.1371/journal.pone.0082860.g004

Table 3. Comparison of biosynthetic metabolites in EtOH or ACR-treated JHH7 and Hc cells determined by CE-TOFMS.

Biosynthetic pathways	Metabolites	KEGG	Fold change			
			EtOH-treated JHH7 vs. Hc		ACR vs. EtOH-treated JHH7	
			Mean	SEM	Mean	SEM
Nucleotide biosynthesis	AMP	C00020	2.50	0.10	0.82	0.00
	ATP	C00002	1.64	0.02	0.72	0.01
	CTP	C00063	1.84	0.11	0.74	0.05
	dATP	C00131	1.26	0.02	0.47	0.07
	dCTP	C00458	2.74	0.06	0.69	0.07
	dTTP	C00459	1.96	0.04	0.61	0.06
	GDP	C00035	2.76	0.15	0.82	0.02
	GTP	C00044	1.67	0.11	0.74	0.04
	IMP	C00130	2.33	0.11	0.71	0.08
	PRPP	C00119	0.68	0.08	0.53	0.11
	Ribulose 5-P	C00199	0.46	0.05	0.68	0.05
	UDP	C00015	2.81	0.05	0.82	0.05
	UTP	C00075	1.22	0.04	0.68	0.02
Amino acid biosynthesis	Ala	C00041	9.23	0.31	0.79	0.02
	Asp	C00049	3.23	0.08	0.77	0.01
	Glu	C00025	1.38	0.02	0.76	0.01
	Gly	C00037	0.64	0.02	0.82	0.01
	Ile	C00407	0.80	0.03	0.79	0.01
	Leu	C00123	0.73	0.03	0.78	0.02
	Lys	C00047	1.94	0.06	0.77	0.03
	Phe	C00079	0.69	0.02	0.78	0.01
	Ser	C00065	5.31	0.20	0.81	0.02
	Thr	C00188	1.94	0.07	0.77	0.00
	Trp	C00078	0.06	0.00	0.78	0.02
	Tyr	C00082	0.71	0.03	0.79	0.02
	Val	C00183	0.83	0.04	0.78	0.02
Lipid biosynthesis	3-Hydroxybutyric acid	C01089	1.58	0.03	0.82	0.03
	DHAP	C00111	0.28	0.03	0.52	0.03

doi:10.1371/journal.pone.0082860.t003

receptors (PPARs) and summarizes the effects of ACR on ATP production was generated using IPA (Figure 7B).

Discussion

The war on cancer has continued for more than 40 years, but the gains have been limited. One potential reason for this limited success that typical drug development in oncology has focused on targets that are essential for the survival of all dividing cells, leading to narrow therapeutic windows [31]. Recent advances in metabolite profiling methodologies have generated an alternative window for cancer therapy in targeting cancer metabolism [13]. ACR, a very promising drug that is currently in clinical trials for HCC treatment, has been shown to markedly prevent the recurrence of HCC [3] and selectively inhibit HCC cell growth [5]. We have previously exploited the potential target molecules of ACR that are associated with the promotion of tumor cell proliferation [5] or angiogenesis [32]. In this study, we performed metabolome analyses in JHH7 and Hc cells treated with ACR using both NMR and CE-TOFMS technologies to further understand the molecular pathways that underlie the cancer-selective growth suppressive effect of ACR. We found that ACR selectively suppressed the enhanced nucleotide synthesis and energy metabolism of HCC cells, suggesting that metabolic pathways may be important targets for ACR's anti-cancer activity. The further study of these pathways will benefit the development of more effective cancer drugs and therapies against HCC.

Generally, the metabolic patterns of JHH7 and Hc cells were almost completely opposite to each other (Figure 2), which is consistent with previous reports that cancer cells exhibit considerably different metabolic requirements than most normal differentiated cells and supports the hypothesis that cancer may be a type of metabolic disease [33]. Although the primary cause of cancer is assumed to be at the level of gene expression, metabolites can be considered to be the end products of the cellular regulatory processes that underlie malignant cell growth such as genome instability and mutability [34]. Metabolomic comparison of HCC and control liver tissues have been carried out in several animal and human studies aiming to define metabolomic biomarkers for the early detection of HCC [35,36]. In this study, the abundance

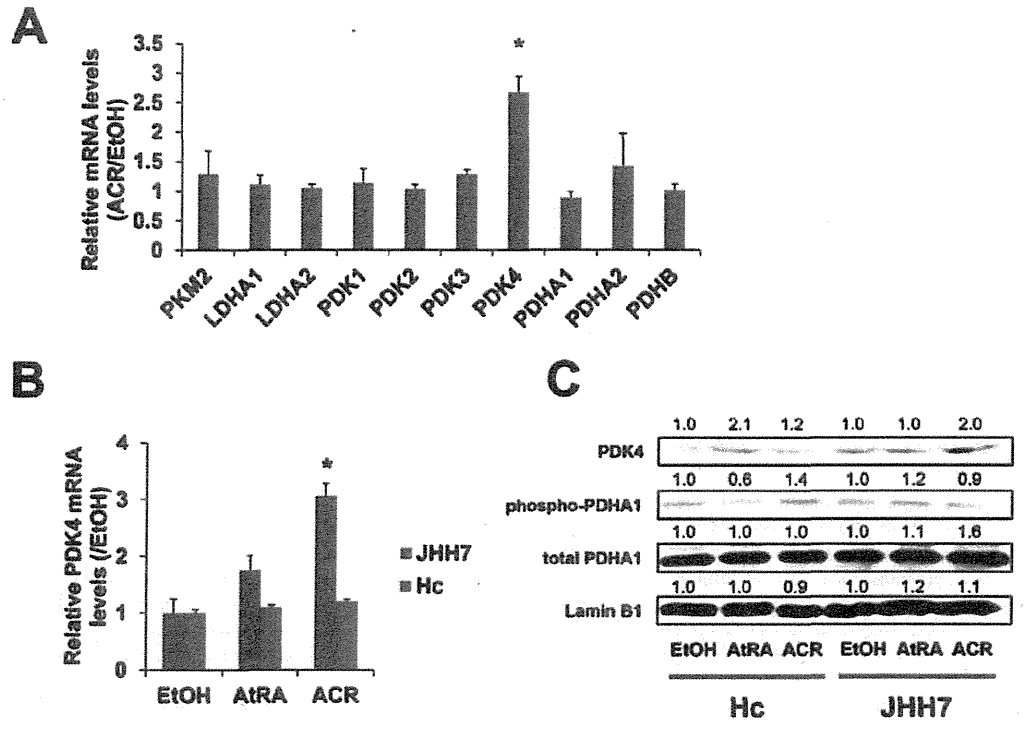

Figure 5. ACR increase the expression of PDK4 in JHH7 cells but not Hc cells. The effect of ACR on the expression of genes related to energy metabolism and ATP production in cancer cells (*A*). Levels of PDK4 mRNA (*B*) and levels of PDH4, phospho-PDHA1 and total PDHA1 protein (*C*) in JHH7 and Hc cells treated with EtOH, AtRA and ACR. The statistical significance of difference was evaluated using the Student's *t*-test.
doi:10.1371/journal.pone.0082860.g005

of 71 metabolites was found to be significantly different between JHH7 and Hc cells; 49 of these metabolites were significantly down-regulated by ACR in JHH7 cells (Figure 2 and Table S2). It is not unexpected that an IPA analysis revealed that most of these metabolites are involved in the amino acids and nucleotide biosynthetic pathways, such as "tRNA Charging", "Purine Nucleotides De Novo Biosynthesis II" and "Pyrimidine Ribonucleotides De Novo Biosynthesis" (Tables 2 and 3). It is well known that cancer cell metabolism must provide a large increase in lipid, protein, and nucleotide synthesis (biomass) to support their uncontrolled high rate of cell growth and proliferation [13]. Our findings indicate that ACR may exert its anti-cancer effect by blocking the biosynthetic processes of cancer cells. Interestingly, a bioinformatics-based anticancer drug screening program in Japan revealed that ACR shares similar anticancer activity pattern with the antipyrimidine drugs doxifluridine and cytarabine and an antipurine drug, 6-mercaptopurine, as assayed by growth inhibition against a panel of 39 human cancer cell lines (JFC39) [37,38,39].

ATP is the main energy source for the majority of cellular functions, and impaired cellular energy metabolism is the defining characteristic of nearly all cancers regardless of cellular or tissue

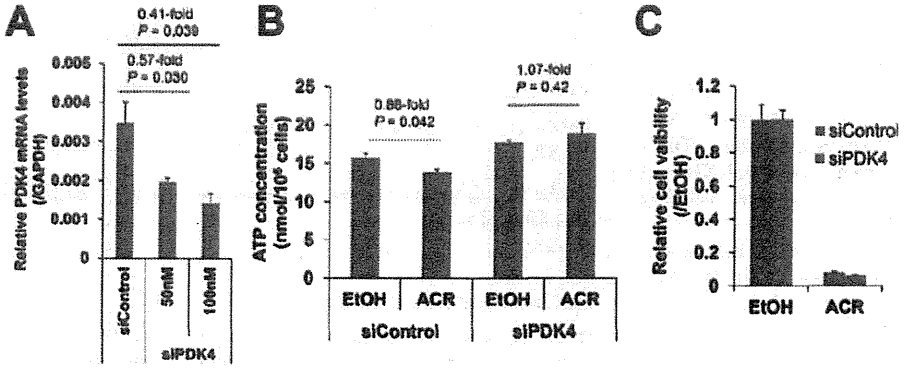

Figure 6. Functional analysis of PDK4 in JHH7 cells. The effect of siPDK4 on PDK4 gene expression (*A*). The effect of 50 nM siPDK4 on the ACR-mediated cellular ATP levels (*B*) and the proliferation (*C*) of JHH7 cells.
doi:10.1371/journal.pone.0082860.g006

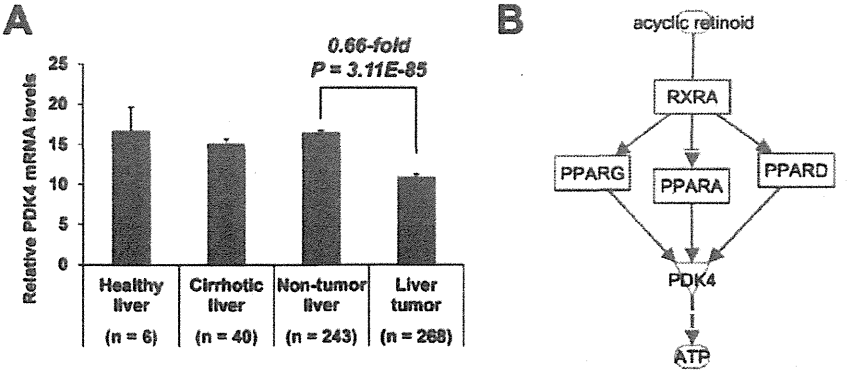

Figure 7. Clinical expression levels of PDK4. The expression of PDK4 mRNA in human liver cancer (GEO data set GSE25097) (*A*). Statistical significance was evaluated using the Mann-Whitney U test. A schematic model of the PDK4-denpendent regulatory network of ACR on ATP production in JHH7 cells generated using IPA (*B*).
doi:10.1371/journal.pone.0082860.g007

origin [33]. Of particular interest, ACR can selectively inhibit the production of ATP in JHH7 cells but not in Hc cells (Figure 4). It has been proven that chemical depletion of ATP can inhibit the growth of HCC cells [40]. This may partially explain the cancer-selective growth suppression effect of ACR. To further understand the molecular signaling mechanisms that underlie this effect, we examined the effect of ACR on the expression of energy production-related genes and observed that the expression of PDK4 was significantly enhanced by ACR in JHH7 cells but not in Hc cells (Figure 5). PDK4 is a key regulator of tricarboxylic acid (TCA) cycle; PDK4 phosphorylates and inactivates the pyruvate dehydrogenase (PDH) complex and thereby switches the energy source for the production of ATP from glucose to fatty acids. Although the cellular pyruvate level was not detected by CE-TOFMS and no effect of ACR was found on the phosphorylation of PDHA1 by western blot analysis (Figure 5C), the knockdown of PDK4 expression using RNA interference in JHH7 cells can rescue the decreased cellular ATP levels induced by ACR (Figure 6B), suggesting that PDK4 may be an important feature of ACR's anti-cancer activity. Moreover, we performed data mining using the GEO database and found that PDK4 expression is significantly down-regulated in liver tumors compared to adjacent non-tumor liver tissues (Figure 7A). The role of PDK4 in cancer therapy is complex; the inhibition of PDK4 is sufficient to inhibit the proliferation of and induce apoptosis in lung cancer cells [41], but the overexpression of PDK4 is also able to decrease ATP levels and suppress de novo lipogenesis and proliferation in breast cancer cells [30]. The specific role of PDK4 in HCC remains to be fully determined. Our results suggest that PDK4 up-regulation has a suppressive effect on HCC. Consistent with this implication, the results of IPA analysis suggest that the cancer-selective, growth-suppressive effect of ACR in inhibiting the ATP production of HCC cells may be related to a putative PDK4-dependent molecular signaling mechanism involving RXR and PPARs, as has been reported in certain fatty acid signaling pathways [42] (Figure 7B).

Although the Warburg effect is a well-recognized hallmark of cancer metabolism, it remains controversial [43]. Warburg hypothesized that tumor cells convert most of their glucose to lactate due to mitochondrial defects. However, subsequent studies showed that most tumor mitochondria are not defective in their ability to carry out oxidative phosphorylation [43]. In fact, we propose that mitochondrial oxidative phosphorylation may be important in supporting HCC cell proliferation based on the following observations: 1) the content of lactate, the major end product of glycolysis, is lower in JHH7 cells than in Hc cells (0.40-fold, Table S2) and 2) ACR up-regulates the expression of PDK4, which attenuates the flux of glycolytic carbon into mitochondrial oxidation and can reduce the production of ATP and inhibit the growth of JHH7 cells.

In summary, our study is the first to investigate the effect of ACR on cancer cell metabolism. A comparison of the metabolic effects of ACR in JHH7 and Hc cells was performed, and a JHH7-selective inhibitory effect of ACR on the production of ATP was observed. The underlying molecular signaling mechanism may relate in part to the cancer-selective enhancement of PDK4 expression, suggesting that mitochondrial oxidative phosphorylation is important in the energy metabolism of HCC cells. However, it should be noted that although PDK4 knockdown can rescue the decreased cellular ATP levels induced by ACR, no effect was observed on the inhibitory effect of ACR on the proliferation of JHH7 cells. Further research is needed to combine the cancer-selective metabolic pathways identified in this study and other signaling pathways to increase our knowledge of ACR's selective anti-cancer activity and to develop more effective cancer drugs and therapies to help us win the war against HCC.

Supporting Information

Figure S1 Statistical analysis of metabolites in JHH7 cells detected by ^{1}H-NMR. PCA score plots of the NMR spectra of JHH7 cells treated with EtOH or 10 μM ACR for 4 h and 18 h (*A*) or only 18 h (*B*).
(PPTX)

Table S1 The primers used in this study.
(XLSX)

Table S2 Quantification of major metabolites in JHH7 and Hc cells.
(XLSX)

Author Contributions

Conceived and designed the experiments: XYQ MT MS HM SK. Performed the experiments: XYQ FW. Analyzed the data: XYQ. Contributed reagents/materials/analysis tools: NI. Wrote the paper: XYQ SK.

References

1. Venook AP, Papandreou C, Furuse J, de Guevara LL (2010) The incidence and epidemiology of hepatocellular carcinoma: a global and regional perspective. Oncologist 15 Suppl 4: 5–13.
2. Llovet JM, Schwartz M, Mazzaferro V (2005) Resection and liver transplantation for hepatocellular carcinoma. Semin Liver Dis 25: 181–200.
3. Muto Y, Moriwaki H, Ninomiya M, Adachi S, Saito A, et al. (1996) Prevention of second primary tumors by an acyclic retinoid, polyprenoic acid, in patients with hepatocellular carcinoma. Hepatoma Prevention Study Group. N Engl J Med 334: 1561–1567.
4. Muto Y, Moriwaki H, Saito A (1999) Prevention of second primary tumors by an acyclic retinoid in patients with hepatocellular carcinoma. N Engl J Med 340: 1046–1047.
5. Tatsukawa H, Sano T, Fukaya Y, Ishibashi N, Watanabe M, et al. (2011) Dual induction of caspase 3- and transglutaminase-dependent apoptosis by acyclic retinoid in hepatocellular carcinoma cells. Mol Cancer 10: 4.
6. Obora A, Shiratori Y, Okuno M, Adachi S, Takano Y, et al. (2002) Synergistic induction of apoptosis by acyclic retinoid and interferon-beta in human hepatocellular carcinoma cells. Hepatology 36: 1115–1124.
7. Okada H, Honda M, Campbell JS, Sakai Y, Yamashita T, et al. (2012) Acyclic retinoid targets platelet-derived growth factor signaling in the prevention of hepatic fibrosis and hepatocellular carcinoma development. Cancer Res 72: 4459–4471.
8. Shao RX, Otsuka M, Kato N, Taniguchi H, Hoshida Y, et al. (2005) Acyclic retinoid inhibits human hepatoma cell growth by suppressing fibroblast growth factor-mediated signaling pathways. Gastroenterology 128: 86–95.
9. Kagawa M, Sano T, Ishibashi N, Hashimoto M, Okuno M, et al. (2004) An acyclic retinoid, NIK-333, inhibits N-diethylnitrosamine-induced rat hepatocarcinogenesis through suppression of TGF-alpha expression and cell proliferation. Carcinogenesis 25: 979–985.
10. Matsushima-Nishiwaki R, Okuno M, Takano Y, Kojima S, Friedman SL, et al. (2003) Molecular mechanism for growth suppression of human hepatocellular carcinoma cells by acyclic retinoid. Carcinogenesis 24: 1353–1359.
11. Suzui M, Masuda M, Lim JT, Albanese C, Pestell RG, et al. (2002) Growth inhibition of human hepatoma cells by acyclic retinoid is associated with induction of p21(CIP1) and inhibition of expression of cyclin D1. Cancer Res 62: 3997–4006.
12. Matsushima-Nishiwaki R, Okuno M, Adachi S, Sano T, Akita K, et al. (2001) Phosphorylation of retinoid X receptor alpha at serine 260 impairs its metabolism and function in human hepatocellular carcinoma. Cancer Res 61: 7675–7682.
13. Vander Heiden MG (2011) Targeting cancer metabolism: a therapeutic window opens. Nat Rev Drug Discov 10: 671–684.
14. Koppenol WH, Bounds PL, Dang CV (2011) Otto Warburg's contributions to current concepts of cancer metabolism. Nat Rev Cancer 11: 325–337.
15. Butler EB, Zhao Y, Munoz-Pinedo C, Lu J, Tan M (2013) Stalling the engine of resistance: targeting cancer metabolism to overcome therapeutic resistance. Cancer Res 73: 2709–2717.
16. El-Serag HB (2012) Epidemiology of viral hepatitis and hepatocellular carcinoma. Gastroenterology 142: 1264–1273 e1261.
17. Welzel TM, Graubard BI, Zeuzem S, El-Serag HB, Davila JA, et al. (2011) Metabolic syndrome increases the risk of primary liver cancer in the United States: a study in the SEER-Medicare database. Hepatology 54: 463–471.
18. Fujise K, Nagamori S, Hasumura S, Homma S, Sujino H, et al. (1990) Integration of hepatitis B virus DNA into cells of six established human hepatocellular carcinoma cell lines. Hepatogastroenterology 37: 457–460.
19. Qin XY, Wei F, Yoshinaga J, Yonemoto J, Tanokura M, et al. (2011) siRNA-mediated knockdown of aryl hydrocarbon receptor nuclear translocator 2 affects hypoxia-inducible factor-1 regulatory signaling and metabolism in human breast cancer cells. FEBS Lett 585: 3310–3315.
20. Wei F, Furihata K, Hu F, Miyakawa T, Tanokura M (2010) Complex mixture analysis of organic compounds in green coffee bean extract by two-dimensional NMR spectroscopy. Magn Reson Chem 48: 857–865.
21. Ohashi Y, Hirayama A, Ishikawa T, Nakamura S, Shimizu K, et al. (2008) Depiction of metabolome changes in histidine-starved Escherichia coli by CE-TOFMS. Mol Biosyst 4: 135–147.
22. Sugimoto M, Hirayama A, Robert M, Abe S, Soga T, et al. (2010) Prediction of metabolite identity from accurate mass, migration time prediction and isotopic pattern information in CE-TOFMS data. Electrophoresis 31: 2311–2318.
23. Qin XY, Akanuma H, Wei F, Nagano R, Zeng Q, et al. (2012) Effect of low-dose thalidomide on dopaminergic neuronal differentiation of human neural progenitor cells: a combined study of metabolomics and morphological analysis. Neurotoxicology 33: 1375–1380.
24. Qin XY, Kojima Y, Mizuno K, Ueoka K, Muroya K, et al. (2012) Identification of novel low-dose bisphenol a targets in human foreskin fibroblast cells derived from hypospadias patients. PLoS One 7: e36711.
25. Bronner IF, Bochdanovits Z, Rizzu P, Kamphorst W, Ravid R, et al. (2009) Comprehensive mRNA expression profiling distinguishes tauopathies and identifies shared molecular pathways. PLoS One 4: e6826.
26. Vander Heiden MG, Lunt SY, Dayton TL, Fiske BP, Israelsen WJ, et al. (2011) Metabolic pathway alterations that support cell proliferation. Cold Spring Harb Symp Quant Biol 76: 325–334.
27. Vander Heiden MG, Cantley LC, Thompson CB (2009) Understanding the Warburg effect: the metabolic requirements of cell proliferation. Science 324: 1029–1033.
28. Levine AJ, Puzio-Kuter AM (2010) The control of the metabolic switch in cancers by oncogenes and tumor suppressor genes. Science 330: 1340–1344.
29. DeBerardinis RJ, Lum JJ, Hatzivassiliou G, Thompson CB (2008) The biology of cancer: metabolic reprogramming fuels cell growth and proliferation. Cell Metab 7: 11–20.
30. Grassian AR, Metallo CM, Coloff JL, Stephanopoulos G, Brugge JS (2011) Erk regulation of pyruvate dehydrogenase flux through PDK4 modulates cell proliferation. Genes Dev 25: 1716–1733.
31. Michelakis ED, Webster L, Mackey JR (2008) Dichloroacetate (DCA) as a potential metabolic-targeting therapy for cancer. Br J Cancer 99: 989–994.
32. Komi Y, Sogabe Y, Ishibashi N, Sato Y, Moriwaki H, et al. (2010) Acyclic retinoid inhibits angiogenesis by suppressing the MAPK pathway. Lab Invest 90: 52–60.
33. Seyfried TN, Shelton LM (2010) Cancer as a metabolic disease. Nutr Metab (Lond) 7: 7.
34. Hanahan D, Weinberg RA (2011) Hallmarks of cancer: the next generation. Cell 144: 646–674.
35. Beyoglu D, Imbeaud S, Maurhofer O, Bioulac-Sage P, Zucman-Rossi J, et al. (2013) Tissue metabolomics of hepatocellular carcinoma: Tumor energy metabolism and the role of transcriptomic classification. Hepatology 58: 229–238.
36. Wang J, Zhang S, Li Z, Yang J, Huang C, et al. (2011) (1)H-NMR-based metabolomics of tumor tissue for the metabolic characterization of rat hepatocellular carcinoma formation and metastasis. Tumour Biol 32: 223–231.
37. Yamori T (2004) [Chemical evaluation by cancer cell line panel and its role in molecular target-based anticancer drug screening]. Gan To Kagaku Ryoho 31: 485–490.
38. (2004) Results of molecular target antineoplastic agents screening. Gan To Kagaku Ryoho 31 Suppl 1: 1–150.
39. Nakatsu N, Nakamura T, Yamazaki K, Sadahiro S, Makuuchi H, et al. (2007) Evaluation of action mechanisms of toxic chemicals using JFCR39, a panel of human cancer cell lines. Mol Pharmacol 72: 1171–1180.
40. Dilip A, Cheng G, Joseph J, Kunnimalaiyaan S, Kalyanaraman B, et al. (2013) Mitochondria-targeted antioxidant and glycolysis inhibition: synergistic therapy in hepatocellular carcinoma. Anticancer Drugs.
41. Bonnet S, Archer SL, Allalunis-Turner J, Haromy A, Beaulieu C, et al. (2007) A mitochondria-K+ channel axis is suppressed in cancer and its normalization promotes apoptosis and inhibits cancer growth. Cancer Cell 11: 37–51.
42. Schoonjans K, Staels B, Auwerx J (1996) Role of the peroxisome proliferator-activated receptor (PPAR) in mediating the effects of fibrates and fatty acids on gene expression. J Lipid Res 37: 907–925.
43. Ward PS, Thompson CB (2012) Metabolic reprogramming: a cancer hallmark even warburg did not anticipate. Cancer Cell 21: 297–308.

Article

Journal of Histochemistry & Cytochemistry 61(11) 793–801

DOI: 10.1369/0022155413501676
jhc.sagepub.com
SAGE

Variations in Both TG1 and TG2 Isozyme-specific In Situ Activities and Protein Expressions during Mouse Embryonic Development

Miho Itoh, Hideki Tatsukawa, Lee Eun-Seo, Kiyofumi Yamanishi, Soichi Kojima, and Kiyotaka Hitomi

Graduate School of Bioagricultural Sciences (MI), and Graduate School of Pharmaceutical Sciences (MI,HT,KH), Nagoya University, Nagoya, Japan; Micro-signaling Regulation Technology Unit, RIKEN Center for Life Science Technologies, Riken ASI, Wako, Saitama, Japan (LES,SK); and Department of Dermatology, Hyogo College of Medicine, Nishinomiya, Hyogo, Japan (KY)

Summary

Transglutaminase (TG) is a family of enzymes that catalyzes cross-linking reactions among proteins. Using fluorescent-labeled highly reactive substrate peptides, we recently developed a system to visualize isozyme-specific in situ enzymatic activity. In the present study, we investigated the in situ activities of TG1 (skin-type) and TG2 (tissue-type) using whole mouse sections of various embryonic developmental stages and neonates. In each case, we also successfully used immunostaining of identical whole mouse sections for protein expression after detection of enzymatic activities. In general, the enzymatic activity was correlated with TG protein expression. However, in some tissues, TG protein expression patterns, which were inconsistent with the enzymatic activities, suggested that inactive TGs were produced possibly by self cross-linking or other modifications. Our method allowed us to simultaneously observe developmental variations in both TG isozyme-specific activities and protein levels in mouse embryonic and neonate tissues. (J Histochem Cytochem 61:793–801, 2013)

Keywords

transglutaminase, calcium, embryo, development

Introduction

Transglutaminases (TGs) are a family of enzymes comprising eight isozymes that are widely distributed in tissues and cells (Griffin et al. 2002; Lorand and Graham 2003). These enzymes are involved in multiple biological processes by catalyzing isopeptide bond formation between proteins through glutamine and lysine residues in substrate proteins. In addition, these enzymes catalyze the post-translational modifications such as polyamination or conversion to glutamic acid by incorporating either a primary amine or a water molecule into the glutamine residues, respectively. Among these family members, TG1 (skin-type) and TG2 (tissue-type) are major isozymes that display epidermal and ubiquitous expressions, respectively.

TG1 plays a central role in the formation of the skin barrier, by cross-linking several structural proteins to form a cornified envelope in the most differentiated keratinocytes (Candi et al. 2005; Eckert et al. 2005; Hitomi 2005). This cornified envelope is a 15-nm-thick structure comprising covalently cross-linked products that are deposited beneath the plasma membrane. Mice lacking the gene for TG1

Received for publication May 4, 2013; accepted July 15, 2013.

Corresponding Author:
Kiyotaka Hitomi, Department of Basic Medicinal Sciences, Graduate School of Pharmaceutical Sciences, Nagoya University, Chikusa, Nagoya 464-8601, Japan.
E-mail: hitomi@ps.nagoya-u.ac.jp